iScience

CellPress

Article

Balanced Activity between Kv3 and Nav Channels Determines Fast-Spiking in Mammalian Central Neurons

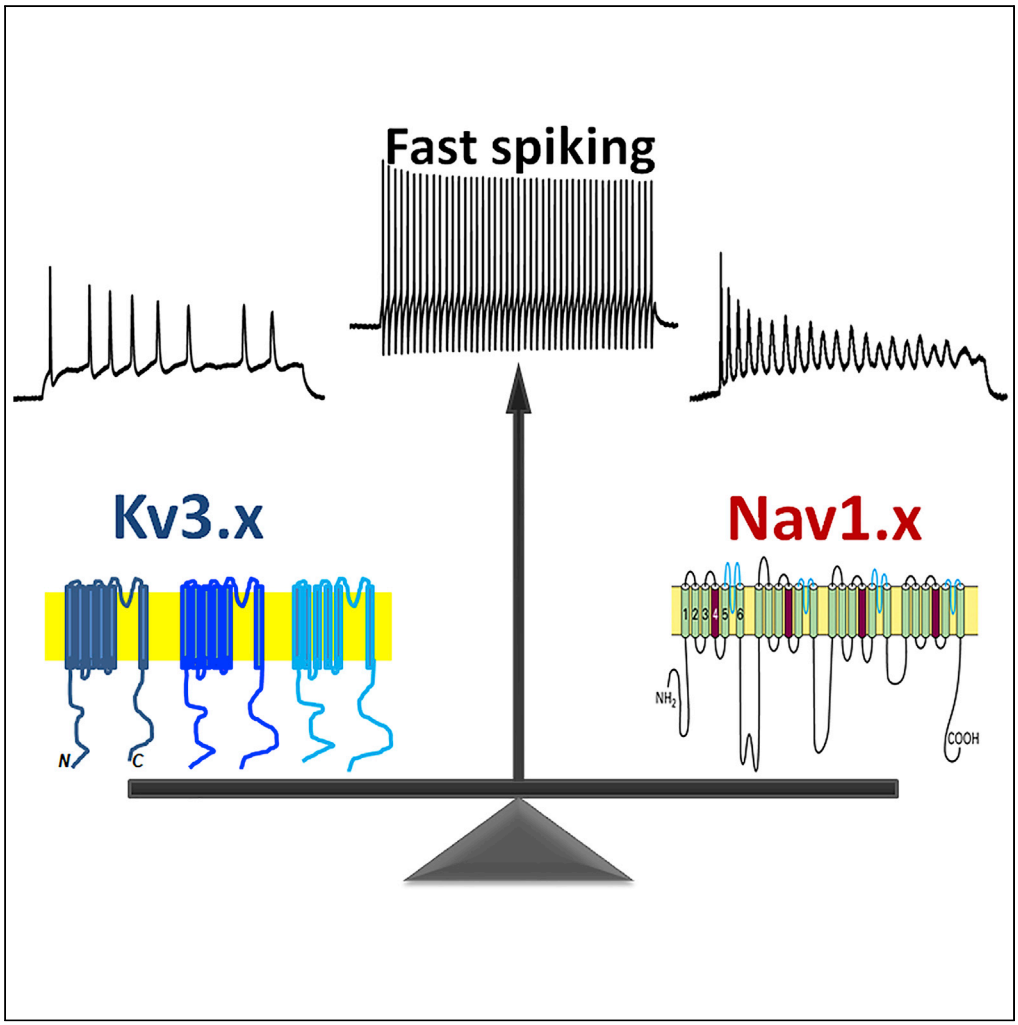

Yuanzheng Gu, Dustin Servello, Zhi Han, Rupa R. Lalchandani, Jun B. Ding, Kun Huang, Chen Gu

gu.49@osu.edu

HIGHLIGHTS

Kv3-induced fast spiking correlates with the amplitude of inward Na^+ current

Kv3 and Nav co-expression converts slow-spiking to fast-spiking with 100% efficiency

The Kv3/Nav mRNA ratio strongly predicts the maximal firing frequency of central neurons

Gu et al., iScience 9, 120–137
November 30, 2018
https://doi.org/10.1016/j.isci.2018.10.014

iScience

CellPress

Article

Balanced Activity between Kv3 and Nav Channels Determines Fast-Spiking in Mammalian Central Neurons

Yuanzheng Gu,[1] Dustin Servello,[2] Zhi Han,[3,4,5] Rupa R. Lalchandani,[6] Jun B. Ding,[6] Kun Huang,[3,5,7] and Chen Gu[1,2,8,*]

SUMMARY

Fast-spiking (FS) neurons can fire action potentials (APs) up to 1,000 Hz and play key roles in vital functions such as sound location, motor coordination, and cognition. Here we report that the concerted actions of Kv3 voltage-gated K^+ (Kv) and Na^+ (Nav) channels are sufficient and necessary for inducing and maintaining FS. Voltage-clamp analysis revealed a robust correlation between the Kv3/Nav current ratio and FS. Expressing Kv3 channels alone could convert ~30%–60% slow-spiking (SS) neurons to FS in culture. In contrast, co-expression of either Nav1.2 or Nav1.6 together with Kv3.1 or Kv3.3, but not alone or with Kv1.2, converted SS to FS with 100% efficiency. Furthermore, RNA-sequencing-based genome-wide analysis revealed that the Kv3/Nav ratio and Kv3 expression levels strongly correlated with the maximal AP frequencies. Therefore, FS is established by the properly balanced activities of Kv3 and Nav channels and could be further fine-tuned by channel biophysical features and localization patterns.

INTRODUCTION

The temporal resolution of human body and mind is determined by the processing speed of related neural circuits in the nervous system. Long-distance transmission of information in the nervous system is mainly encoded by the firing frequency and pattern of propagating action potentials (APs). The maximal frequency of APs is a key physiological feature of mammalian central neurons and a determinant of the computational speed of the neural circuits. Rapid neural computation is essential in many important neurophysiological functions. For instance, vestibulo-ocular reflex is vital for stabilizing images on the retinas during head movement, whereas detection of interaural time difference by auditory neurons allows mammals to determine sound location (Gittis and du Lac, 2006; Vonderschen and Wagner, 2014). The brain contains several types of fast-spiking (FS) neurons, which are capable of firing APs at high frequencies with consistent AP amplitudes and uniform interspike intervals (Bean, 2007; McCormick et al., 1985; Rudy and McBain, 2001). These neurons include cerebellar Purkinje and granule cells, auditory neurons, and parvalbumin-positive (PV+) GABAergic interneurons (underlying γ oscillation) in various brain regions (Barry et al., 2013; Diwakar et al., 2009; Du et al., 1996; Lien and Jonas, 2003; Martina et al., 2007; Wang et al., 1998). In particular, PV+ interneurons are critically involved in advanced computations in neuronal networks of higher brain functions, such as learning and memory, cognition, and emotion (Hu et al., 2014). Disrupted electrical signaling in these FS neurons leads to epilepsy, ataxia, and mental disorders (Catterall et al., 2010; Hu et al., 2014; Lewis et al., 2005; Marin, 2012; Nakazawa et al., 2012; Waters et al., 2006; Zhuchenko et al., 1997). Therefore, it is critical to understand the ionic mechanisms underlying FS induction and regulation under healthy and pathological conditions.

Among all voltage-gated ion channels, Kv3 voltage-gated K^+ (Kv) channels appear to play an important role in FS induction. Their unique biophysical properties, including high activation threshold and rapid activation/deactivation kinetics, allow the neurons to quickly repolarize after Na^+ influx without compromising the inward current and the re-activation of voltage-gated Na^+ (Nav) channels, which leads to the generation of repetitive AP spiking with narrow AP waveforms (see more details in recent review articles Bean, 2007; Kaczmarek and Zhang, 2017; Rudy and McBain, 2001). The Kv3 channel subfamily contains four members, from Kv3.1 to Kv3.4, which are widely expressed in neurons and differ in their biophysical and regulatory properties and expression patterns (Kaczmarek and Zhang, 2017). In particular, Kv3.1 channel is highly expressed in many FS neurons and critical for their high-firing frequency (Barry et al., 2013; Erisir

[1]Department of Biological Chemistry and Pharmacology, The Ohio State University, 182 Rightmire Hall, 1060 Carmack Road, Columbus, OH 43210, USA

[2]Molecular, Cellular and Developmental Biology Graduate Program, The Ohio State University, Columbus, OH 43210, USA

[3]Department of Medicine, Indiana University School of Medicine, Indianapolis, IN 46202, USA

[4]College of Software, Nankai University, Tianjin 300071, China

[5]Regenstrief Institute, Indianapolis, IN 46202, USA

[6]Department of Neurosurgery, and Department of Neurology and Neurological Sciences, Stanford University School of Medicine, Palo Alto, CA, USA

[7]School of Biomedical Engineering, Shenzhen University, Shenzhen 518037, China

[8]Lead Contact

*Correspondence: gu.49@osu.edu

https://doi.org/10.1016/j.isci.2018.10.014

et al., 1999; Espinosa et al., 2004; Gu et al., 2012; Joho et al., 1999; Ozaita et al., 2002; Sekirnjak et al., 1997; Song et al., 2005; Wang et al., 1998). A recent study suggested that the resurgent current of Kv3.1 resulting from a unique combination of steep voltage-dependent gating kinetics and ultra-fast voltage-sensor relaxation is important for FS (Labro et al., 2015). However, expression of Kv3.1 alone could not account for FS firing patterns seen in all neurons. Some FS neurons, for example, cerebellar Purkinje cells, do not express Kv3.1 or Kv3.2, but express Kv3.3 instead (Hurlock et al., 2009). Conversely, some neurons express Kv3.1 and/or Kv3.2 channels but are unable to generate FS, for example, somatostatin-positive (SST+) GABAergic interneurons and retinal starburst amacrine cells (Chow et al., 1999; Cohen, 2001; Ozaita et al., 2004). Therefore, how the expression of Kv3.1 itself or other Kv3 isoforms is related to FS remains unclear.

Resurgent Nav currents have also been implicated in generating rapid and repetitive firing of APs in some neurons (Lewis and Raman, 2014). First identified in Purkinje neurons and later in nearly 20 types of neurons, these resurgent currents can be generated transiently upon repolarization following inactivation (Enomoto et al., 2006; Lewis and Raman, 2014; Magistretti et al., 2006; Raman and Bean, 1997). Among 10 α subunits of Nav channels, Nav1.1, Nav1.2, and Nav1.6 are expressed and play critical roles in the adult mammalian brain (Trimmer and Rhodes, 2004). Expression of Nav1.6 (Cummins et al., 2005; Lewis and Raman, 2014; Raman et al., 1997) and Navβ4, one of the β subunits of Nav channels with only one membrane-spanning segment, are critical for generation of the resurgent currents (Bant and Raman, 2010; Lewis and Raman, 2014; Ransdell et al., 2017). It has been shown that resurgent Nav channels in the open-blocked state are unblocked upon membrane repolarization, leading to "resurgent" Na^+ influx, which contributes to the generation of repetitive high-frequency firing at least in some neurons (Lewis and Raman, 2014).

Two other types of ion channels have been found in FS neurons to regulate their AP firing, including hyperpolarization-activated, cyclic nucleotide-gated cation (HCN) channels and two-pore K^+ leak channel. HCN channels give rise to hyperpolarization-activated currents (I_h) that are carried by a mixture of Na^+ and K^+ and are involved in controlling neuronal rhythmic firing (for more details see a recent review article Biel et al., 2009). Different isoforms of HCN channels are expressed in FS neurons in different CNS regions and likely contribute to the regulation of the firing properties (Aponte et al., 2006; Hughes et al., 2012, 2013). On the other hand, using techniques of microarray, immunohistochemistry, and pharmacology, a recent study showed that the two-pore K^+ leak channels TWIK1 and TASK1 are upregulated during the maturation of neocortical FS GABAergic interneurons, which could lower the input resistance of the neurons to ensure their proper firing features (Okaty et al., 2009).

In addition to the expression levels, the localization of the Nav and Kv3.1 channels also directly affects the maximal AP frequency. The axon initial segment (AIS) is the site where the APs are normally initiated and Nav channels are highly concentrated. The studies of neurons in bird nucleus laminaris encoding interaural time difference for sound localization showed that AISs are shorter and more remote for higher frequency neurons (Kuba et al., 2006, 2010). Our recent studies showed that expression of Kv3.1 channels can convert some SS neurons to FS ones, and an axonally targeted Kv3.1 is more efficient than the dendritically localized Kv3.1 in this process (Gu et al., 2012). However, it is questionable whether FS induction can still be achieved by placing slow-operating channels at the right location alone. Furthermore, based on all previous studies, it is still impossible to rule out that FS can be induced through a previously unrecognized mechanism involving a different ion channel, due to approximately 250 channel genes in the mammalian genome. Taken together, the mechanism that is essential and sufficient for FS induction is still not known.

In the present study, we have obtained several lines of evidence showing that concerted actions of Kv3 and Nav channels are sufficient and necessary for neurons to induce and sustain FS in mammalian neurons. Our experimental results revealed a strong correlation between FS and the balanced activities of these two ion channels. We further demonstrated that expression of Nav channels (Nav1.2 or Nav1.6) with Kv3.1 or Kv3.3, but not alone or with Kv1.2, converted slow-spiking (SS) neurons to FS with 100% efficiency. Finally, we utilized a bioinformatics approach to perform a genome-wide analysis on the expression of Na^+ and K^+ channels. We found that the Kv3/Nav mRNA ratio and Kv3 mRNA levels strongly correlate with the maximal AP frequencies of central neurons. Based on our results, we propose a simplistic model that FS is primarily established by the proper balance of high levels of Kv3 and Nav channels, and further fine-tuned by channel biophysical features and localization patterns.

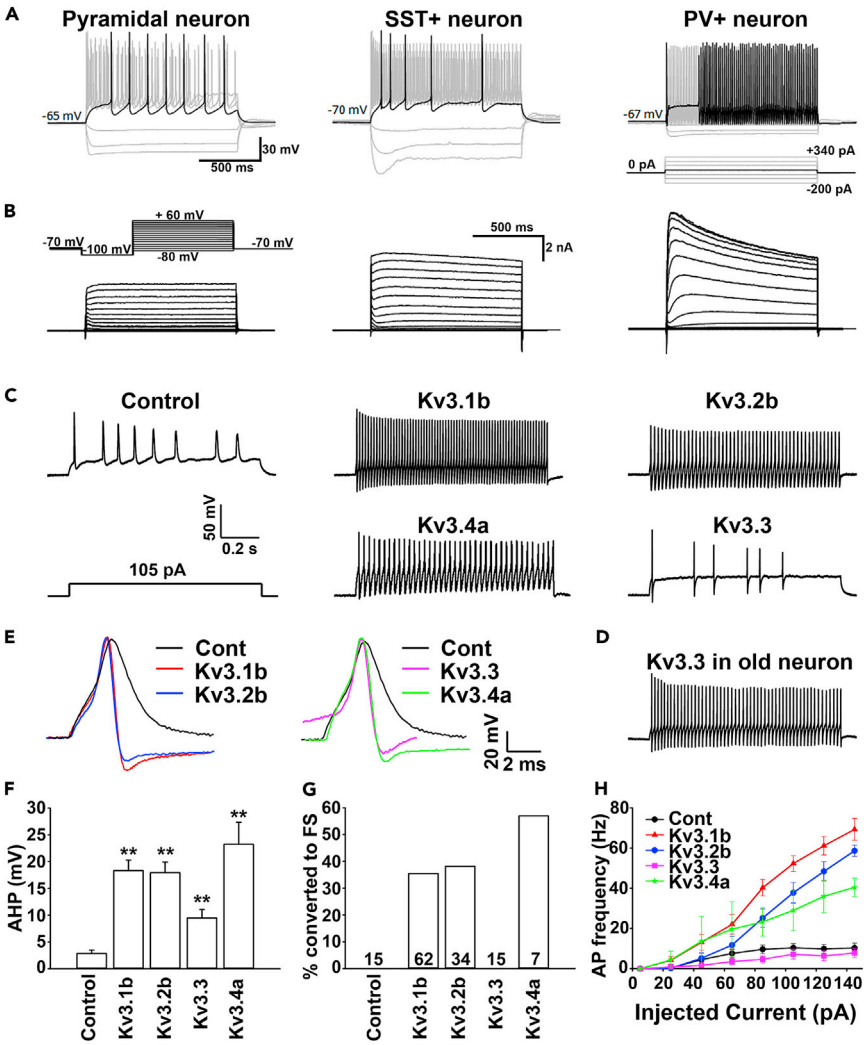

Figure 1. Kv3 Channels Display Different Efficacies in Converting Young SS Neurons to FS

(A) Example AP traces were recorded from pyramidal neuron (left; n = 16), SST+ neuron (middle; n = 15), and PV+ neuron (right; n = 6) in brain slices under current-clamp mode.

(B) The voltage-clamp traces recorded from the same neurons in (A).

(C) Example traces of APs induced by current injection (105 pA; 1 s) in cultured hippocampal neurons (7 DIV) transfected with different Kv3 constructs.

(D) An example trace of APs recorded from older neurons (17 DIV) transfected with Kv3.3.

(E) Waveforms of single APs from transfected young neurons.

(F–H) Summary of the quantification of AP firing recorded from young neurons (7 DIV) transfected with different Kv3 constructs; after-hyperpolarization (AHP) potential (F), % SS neurons converted to FS (G), and the input-output relationship (H). One-way ANOVA followed by Dunnett's test was used in (F). **p < 0.01.

RESULTS

To examine the role of outward Kv currents in FS, we performed current-clamp and voltage-clamp whole-cell recording in identified cortical pyramidal neurons, as well as SST+ and PV+ interneurons, in acute brain slices. Pyramidal neurons were identified by their morphology, and SST+ and PV+ interneurons were identified by the expression of fluorescent protein using SST-Cre;Ai9 and PV-Cre;Ai9 mice. Among all the neurons recorded, PV+ neurons had the highest firing frequency, displayed clear FS phenotype, and had the largest outward Kv currents (Figures 1A and 1B). Approximately one-third of the outward current of PV+ neurons was blocked by a low concentration of 4- aminopyridine (data not shown), confirming the involvement of Kv3 channels. This result is consistent with our previous finding that Kv3.1 expression is

critical for FS (Gu et al., 2012). However, it is yet unknown whether the other three types of Kv3 channels (Kv3.2–Kv3.4) can also induce FS, because Kv3s have different biophysical features and subcellular expression and targeting patterns (Gu and Barry, 2011; Gu et al., 2012; Rudy et al., 1999; Rudy and McBain, 2001).

Distinct Effects of Kv3 Channel Isoforms on Inducing SS Neurons to FS

To compare the effects of expression of different Kv3 isoforms on FS, we transfected cultured hippocampal neurons at 5 days in vitro (DIV) with YFP alone (negative control), Kv3.1b (positive control), Kv3.2b, Kv3.3, or Kv3.4a and performed whole-cell recording 2 days after transfection. For each recorded neuron, we carried out current-clamp recording first to measure the input-output relationship, and then voltage-clamp recording to measure inward and outward currents. At 7 DIV, under the current-clamp mode, we never observed any cultured negative control hippocampal neuron displaying FS. Interestingly, expression of Kv3.1b, Kv3.2b, or Kv3.4a, but not Kv3.3, converted a significant portion of transfected SS neurons into FS with high firing rate, equal amplitude, and interspike interval (Figures 1C–1H). Expression of Kv3 significantly narrowed the AP waveform and increased the amplitude of hyperpolarization (after hyperpolarization [AHP]). The AHP amplitudes were comparable for Kv3.1b, Kv3.2b, and Kv3.4a, whereas the AHP amplitude in neurons expressing Kv3.3 was smaller (Figures 1E and 1F).

Compared with young neurons, the AP amplitude and firing frequency increases in older neurons due to the increased expression of endogenous Nav and Kv channels (Gu et al., 2012). To study whether such conversion is also efficient in mature neurons, we transfected Kv3 constructs into cultured hippocampal neurons at 15 DIV and performed whole-cell recording at 17 DIV. We found that all Kv3 isoforms, including Kv3.3, were able to convert some mature SS neurons (17 DIV) into FS (Figures 1D and S1). Similar to those observed in young neurons, we never observed FS activity from mature hippocampal neurons (17 DIV) without transfection with Kv3s. However, all four Kv3 constructs had similar efficiency in converting mature SS neurons into FS ones (Figure S1). It is worth noting that Kv3 transfection alone is not sufficient for producing FS. A large portion of transfected young and mature neurons (approximately 55%–70%) remained SS despite these neurons also displaying large outward Kv3 currents (Figures 1G and S1D).

Our results are consistent with previous studies showing that either expressing Kv3.1 or injecting Kv3.1-like currents into the SS neurons can partially convert these neurons to FS (Gu et al., 2012; Lien and Jonas, 2003). Our results also demonstrated that, in addition to Kv3.1, other Kv3s could also partially convert neurons from SS to FS.

Quantitative Differences in Biophysical Properties of Kv3 Channel Isoforms

Although Kv3 isoforms overall share similar biophysical properties (compared with other Kv channels), such as high activation threshold and fast activation and deactivation kinetics (Rudy et al., 1999; Rudy and McBain, 2001), so far only Kv3.1 channel was previously shown to be partially sufficient for the SS-FS conversion (Gu et al., 2012; Lien and Jonas, 2003). It is possible that certain Kv3 isoforms, such as Kv3.1, may be more effective than others in FS induction. Indeed, we observed that Kv3.3 expression failed to induce FS in young cultured neurons (Figure 1C), but surprisingly all Kv3s were capable of converting a proportion of mature SS neurons into FS. Our results indicate that the biophysical properties of the four Kv3 isoforms may differentially affect the ability to generate FS firing patterns. To investigate the key biophysical property for FS firing, we performed voltage-clamp recording on HEK293 cells transfected with different Kv3 constructs, including Kv3.1b, Kv3.2b, Kv3.3, and Kv3.4a. These four constructs should represent all Kv3 channels in terms of biophysical properties, because the C-terminal alternative splicing does not affect the biophysical properties of Kv3 channels (Gu et al., 2012; Rudy et al., 1999). All four constructs were efficiently expressed in HEK293 cells and produced large currents that were sufficient for kinetic analysis (Figures 2A–2C). Consistent with previous findings, inactivation was observed with Kv3.3 and Kv3.4a (Figure 2A). Voltage-conductance relationship was similar in Kv3.1b, Kv3.2b, and Kv3.4a, except Kv3.3, which had a steeper slope (Figure 2D). Kv3.2b and Kv3.3 had slower activation kinetics than those of Kv3.1b and Kv3.4, whereas Kv3.4a and Kv3.2b had slower deactivation kinetics than those of Kv3.1b and Kv3.3 (Figures 2E and 2F). Interestingly, Kv3.2b expressed in HEK293 cells displayed a wide range in activation time constant, but not in deactivation time constant (Figures 2G and 2H). In some cells, activation of Kv3.2b channels was very slow (Figure 2G), with activation time constant between 2.4 and 3.6 ms, even slower than that of Kv1.2. However, Kv3.2 expression was quite effective in FS induction in both young and mature neurons (Figures 1 and S1). The voltage-clamp results of Kv3.3 in HEK293 cells did not clearly reveal why Kv3.3 was effective in FS induction in mature neurons but not in young neurons.

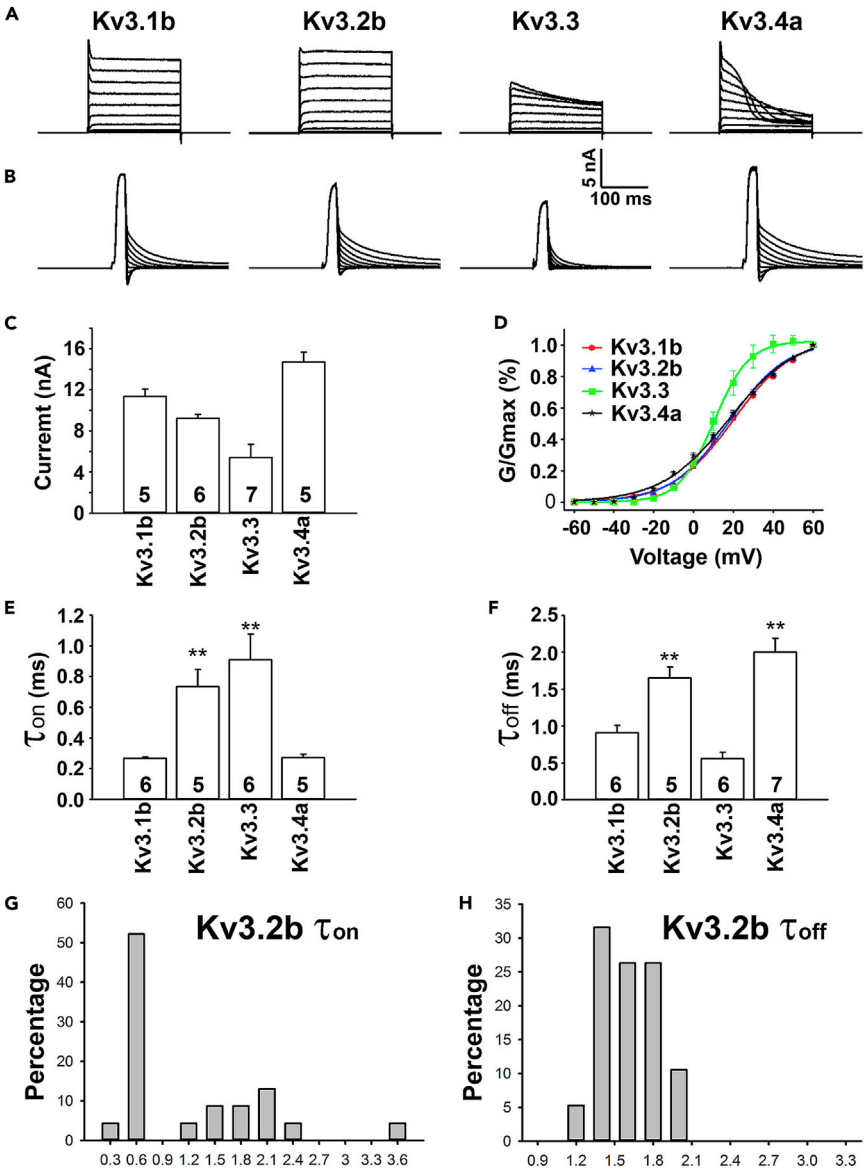

Figure 2. Biophysical Properties of Four Kv3 Channels

Two days after transfection, HEK293 cells that were transfected with Kv3.1b, Kv3.2b, Kv3.3a, or Kv3.4a were recorded with the voltage-clamp mode.

(A) Voltage-clamp recording traces.

(B) Tail currents of different Kv3 constructs.

(C) Summary of current amplitude in HEK293 cells.

(D) The conductance-voltage relationship of the four Kv3 channels.

(E) Activation time constant (τ_{on}) at +30 mV.

(F) Deactivation time constant (τ_{off}).

(G) The range of Kv3.2b τ_{on}.

(H) The range of Kv3.2b τ_{off}; n = 25.

One-way ANOVA followed by Dunnett's test was used in (E) and (F). **$p < 0.01$.

Inward and Outward Currents in FS and SS Neurons

Although voltage-clamp recording of HEK293 cells can accurately reveal biophysical properties of Kv3 channels without the space-clamp issue associated with similar recordings with neurons, HEK293 cells and neurons may possess different endogenous factors that regulate Kv3 channel function. To determine

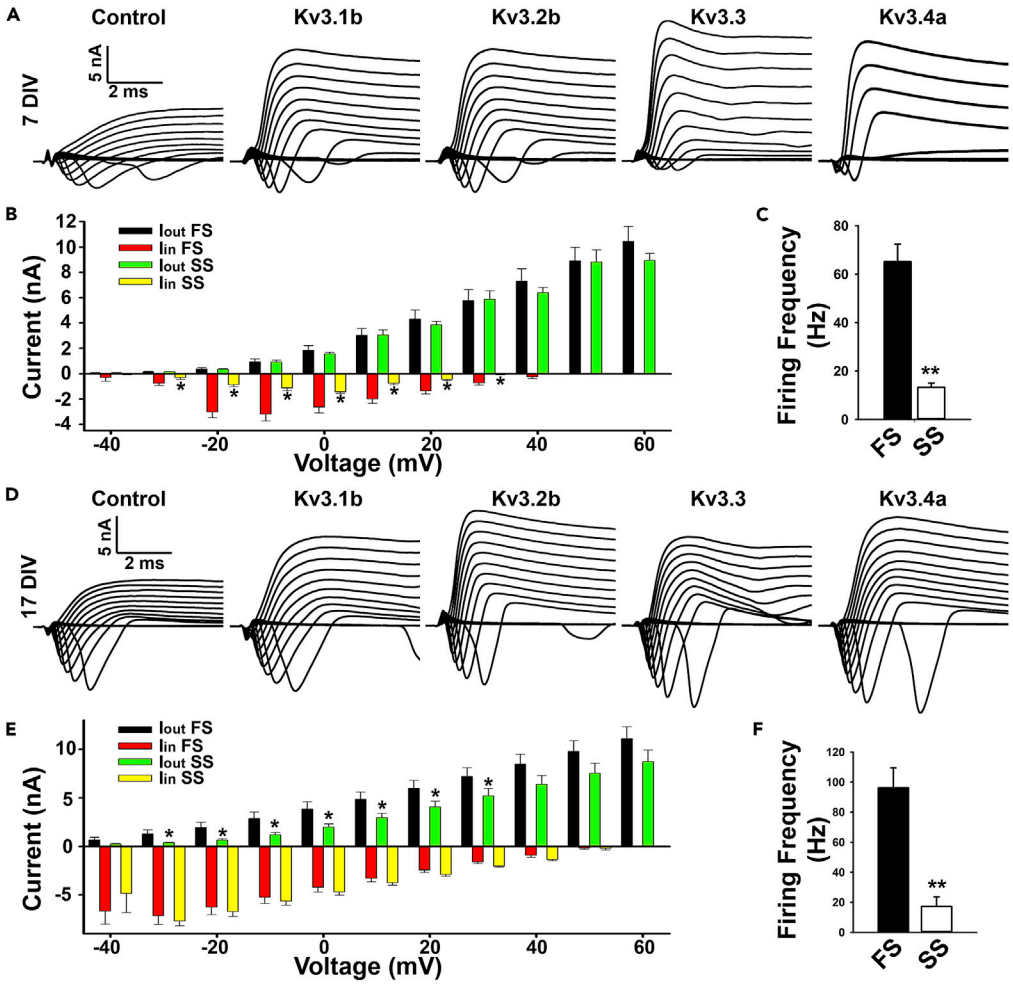

Figure 3. Inward and Outward Currents in SS and FS Neurons That Were Transfected with Kv3 Channels

(A) Example traces of voltage-clamp recording (within the initial 6 ms) from young neurons (7 DIV) transfected with different Kv3 constructs.

(B) Summary of peak I_{out} and I_{in} from SS and FS neurons measured from the traces in each voltage command (from −40 to 60 mV with 10-mV increment).

(C) The average maximal firing frequencies of SS (n = 41) and FS (n = 38) neurons at 7 DIV.

(D) Example traces of voltage-clamp recording (within the initial 6 ms) from old neurons (17 DIV) transfected with different Kv3 constructs.

(E) Summary of peak I_{out} and I_{in} from SS (n = 40) and FS (n = 37) neurons measured from the traces in each voltage command (from −40 to 60 mV with 10-mV increment).

(F) The average maximal firing frequencies of SS and FS neurons at 17 DIV.

Unpaired t test was used. *$p < 0.05$, **$p < 0.01$.

the ionic conductance that may affect FS in neurons, we compared the inward (I_{in}) and outward (I_{out}) currents recorded under the voltage-clamp mode between FS and SS neurons (Figures 3 and S2). Figures 3A and 3D demonstrated the representative recording traces of I_{in} and I_{out} during the initial 6-ms period after current injection (see Figure S2 for the whole current traces with 200-ms voltage command). Neurons with very low I_{out}, which was similar to the I_{out} of untransfected neurons, may not express exogenous Kv3 constructs and therefore were excluded from analysis. In young neurons (7 DIV) transfected with any of the four Kv3 constructs, converted FS neurons and remaining SS neurons were pooled into two groups (FS versus SS). All these neurons (both SS and FS) displayed large Kv3-like outward currents, indicating good transfection efficiency. The peaks of inward and outward current traces were measured for the two groups of neurons and are shown in bar graphs for each voltage episode (Figure 3B). These measured values (I_{in} and I_{out}) were peak inward and outward currents, representing Nav and Kv currents, respectively,

because of temporal segregation of the two currents. It is important to note that these values are still mixtures due to incomplete segregation. Moreover, I_{in} values were often measured when large Nav currents might not be completely clamped. Nonetheless, these values of I_{in} and I_{out} were recorded under defined experimental conditions and are cautiously used in this article. Interestingly, whereas there was no difference in I_{out} between FS and SS, the SS neurons had significantly smaller I_{in} compared with the FS neurons (Figure 3B). In Kv3.3-expressing young neurons, I_{in} was quite small (Figure 3A). Overall, the larger I_{in} appeared to highly correlate with high firing frequencies (Figures 3A–3C) in young neurons.

We performed the same analysis with mature hippocampal neurons at 17 DIV and found that converted FS neurons correlated with significantly larger I_{out} compared with SS neurons (Figures 3D–3F), which is different from young neurons (Figures 3A and 3B). Compared with young (7 DIV) neurons, mature (17 DIV) neurons had significantly larger endogenous inward currents, which were similar in both FS and SS neuron groups (Figures 3D and 3E). It appeared that the amount of I_{out} determined the FS or SS phenotype in mature neurons (Figures 3D–3F). The variation of I_{out} amplitude likely resulted from varied expression efficiency and membrane targeting of channel proteins in different neurons. Taken together, these results indicate that the proper ratio between Nav and Kv3 currents is essential for FS induction.

Concerted Actions of Kv3 and Nav Channels Are Sufficient for FS Induction

To determine whether over-expression of Nav channels can induce FS, we transfected young neurons with Nav1.2 or Nav1.6 constructs and performed whole-cell recording (Figures 4A and 4E). Both Nav1.2 and Nav1.6 are expressed in the CNS (Vacher et al., 2008). In particular, Nav1.6 is a candidate channel for resurgent Na^+ currents (Cummins et al., 2005; Lewis and Raman, 2014; Raman et al., 1997). Over-expressing either Nav1.2 or Nav1.6 in cultured hippocampal neurons at 7 DIV failed to induce FS in any neuron, although their expression was confirmed by markedly increased (>150%) inward currents recorded under the voltage-clamp mode (Figures 4A, 4E, and S3). Thus, increasing Nav current alone does not induce FS.

To determine whether co-expression of any isoform of Nav and Kv3 channels can induce FS, we co-transfected the neurons with Nav1.2 or Nav1.6 and Kv3.1b or Kv3.3. Together with Kv3.1b or Kv3.3, either Nav1.2 or Nav1.6 significantly increased the maximal firing frequencies and induced FS in every transfected neuron (Figure 4). In contrast, when co-expressed with YFP-Kv1.2, both Nav1.2 and Nav1.6 failed to convert SS young neurons into FS (Figures 4D, 4H, and 4I–4K). Voltage-clamp recording confirmed significantly increased inward and outward currents in these neurons that were co-transfected with Nav and Kv3 constructs (Figures 4 and S3). Although Kv3.1b and Kv3.3 differ in FS conversion in young neurons (Figure 2), they behaved indistinguishably in the presence of Nav1.2 or Nav1.6 (Figure 4), suggesting that the failure of FS induction by Kv3.3 in young neuron might mainly result from inadequate endogenous Nav currents. Therefore, our results revealed that co-expression of Nav and Kv3 channels induce FS with 100% efficiency. Moreover, although Nav1.6 itself was not sufficient to induce FS, it appeared that Nav1.6 could induce a higher firing frequency when co-expressed with YFP-Kv1.2, compared with Nav1.2 (Figure 4). Furthermore, the input-output relationship indicates that Nav1.6 appears to be more effective in increasing the AP firing frequency at low injection currents in the presence of Kv3.1b or Kv3.3 (Figures 4I and 4J).

Axon-Dendrite Targeting of Kv3 Channels in FS Induction

To determine whether axon-dendrite targeting of the four Kv3 channel isoforms plays a key role in inducing and maintaining FS, we performed immunostaining for expressed Kv3 and endogenous Nav channels. Our previous studies showed that the two splice variants of Kv3.1, Kv3.1a and Kv3.1b, are mainly targeted to dendritic and axonal membranes, respectively, which fine-tunes the maximal firing frequency (Gu et al., 2012; Xu et al., 2007). Using non-permeabilized staining with an anti-hemagglutinin (HA) antibody, we examined the localization patterns of surface Kv3.1aHA and Kb3.1bHA, and compared them with those of endogenous Nav channels at the AIS (Figures 5A and 5B). Importantly, there were more Kv3.1bHA than Kv3.1aHA at the AIS, colocalizing with endogenous pan Nav channels (Figures 5A and 5B), which is consistent with the fact that Kv3.1bHA can induce higher maximal frequency of AP firing. Nav1.2 is the subunit that expresses at the early developmental stage. Transfection of Kv3.3, but not Kv3.1bHA, Kv3.2b, and Kv3.4aHA, at 5 DIV, significantly reduced the overall levels of Nav1.2 at soma at 7 DIV (Figures 5C and 5D). This explains at least in part why Kv3.3 channel expression failed to convert any young neuron into an FS one (Figure 1). In contrast, over-expression of Kv3 channel constructs in mature neurons did not significantly change the expression level of endogenous Nav channels. Hippocampal neurons at 14 DIV were transfected with Kv3.1b, Kv3.2b, Kv3.3, or Kv3.4a and stained at 16–17 DIV. All these Kv3 channel

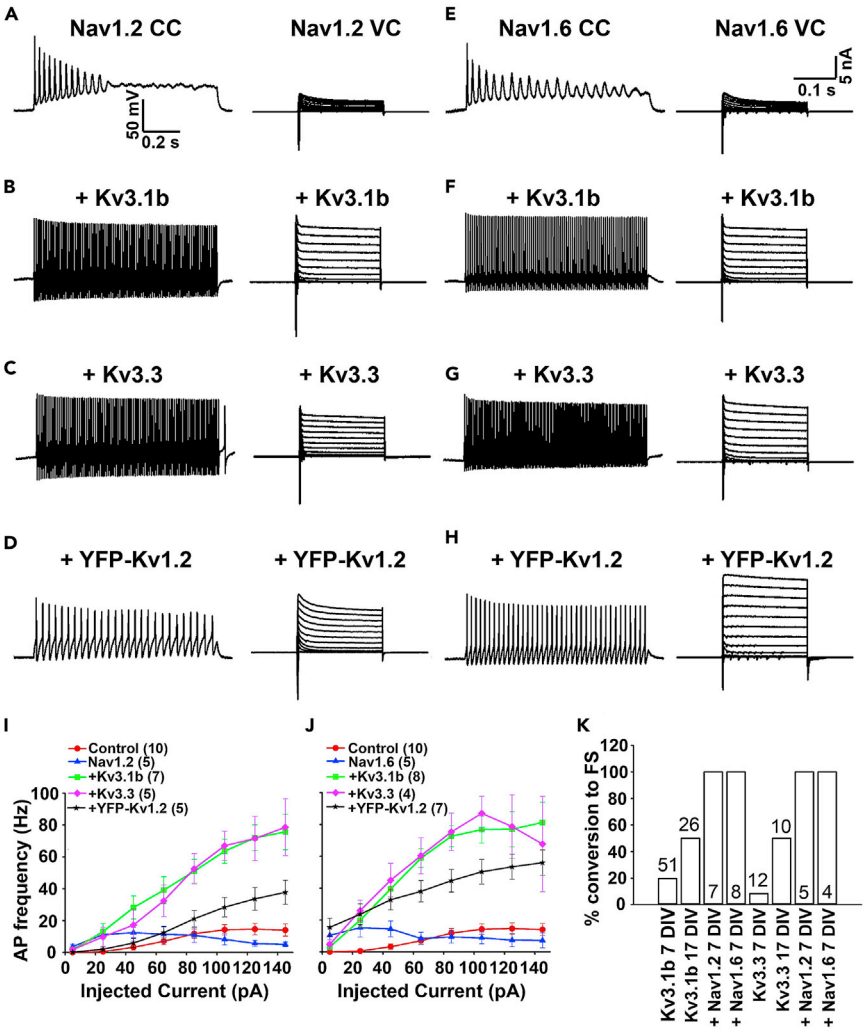

Figure 4. Concerted Action of Nav and Kv3 Channels Is Completely Sufficient for FS Induction

This experiment was carried out in young neurons (7 DIV).

(A–D) Example traces of current-clamp (CC, left) and voltage-clamp (VC, right) recordings that were carried out in neurons transfected with Nav1.2 alone (A), or plus Kv3.1b (B), Kv3.3 (C), or YFP-Kv1.2 (D).

(E–H) Example traces of current-clamp (CC, left) and voltage-clamp (VC, right) recordings that were carried out in neurons transfected with Nav1.6 alone (E), or plus Kv3.1b (F), Kv3.3 (G), or YFP-Kv1.2 (H).

(I) The input-output relationship of neurons transfected with Nav1.2 and others.

(J) The input-output relationship of neurons transfected with Nav1.6 and others.

(K) Summary of percentage of neurons converted into FS under different conditions.

constructs were expressed well in mature neurons (Figures 5E–5H). Their total proteins were present in soma, dendrites, and axons, as well as at the AIS colocalizing with endogenous Nav channels (Figures 5E–5H).

Our recent studies indicate that both Kv3.1b and Nav1 channels bind to ankyrin-G (AnkG) at the AIS, although the functional consequences are different (Barry et al., 2014; Xu et al., 2007). To determine how AnkG might affect the balance of the two channels, we co-expressed Kv3.1b and Nav1.6 with or without AnkG short hairpin RNA vector (AnkGsiR) into young hippocampal neurons and performed current- and voltage-clamp recordings. In the presence of AnkGsiR, Kv3.1b and Nav1.6 failed to induce FS, likely due to the markedly reduced inward current (Figure 6). In contrast, the reduction of outward Kv3 currents was insignificant (Figure 6). Thus, AnkG differentially regulates membrane targeting of the two channels and may be involved in their imbalanced activity.

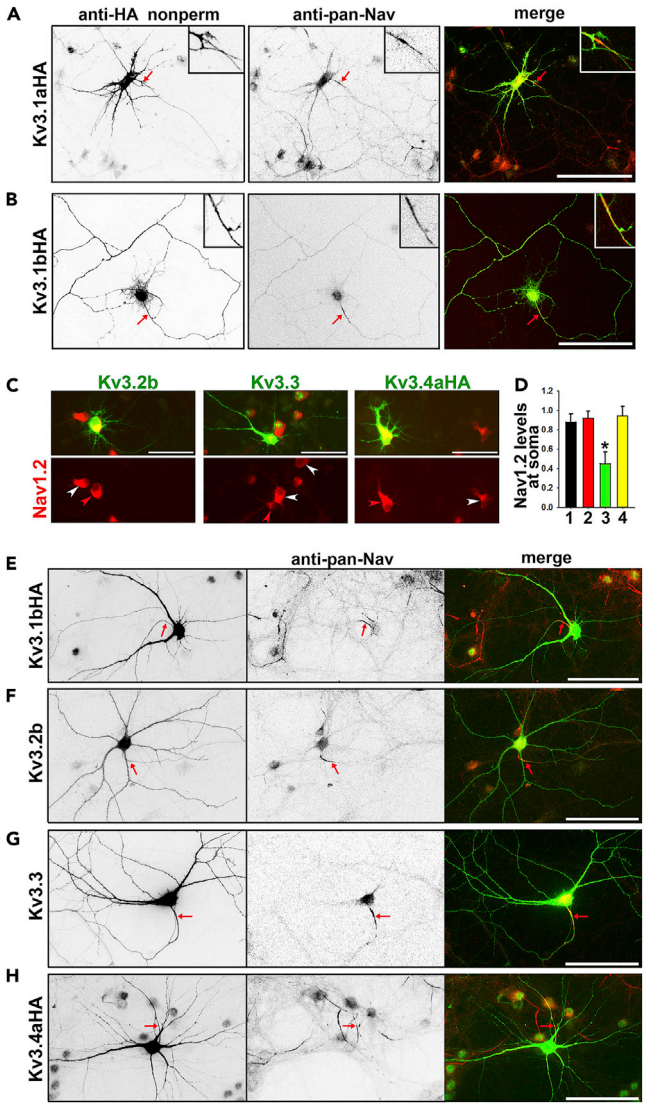

Figure 5. Subcellular Localization Patterns of Nav and Different Kv3 Channels

(A and B) In young neurons (7 DIV), localization of surface Kv3.1aHA (A) and Kv3.1bHA (B) versus endogenous pan-Nav channels was examined. Anti-HA staining was performed under non-permeabilized condition. The AIS (red arrows) is shown in the insets at the top right corners.

(C) Expression of Kv3.2b (green), Kv3.3 (green), and Kv3.4aHA (green) in young neurons differentially changed the endogenous level of Nav1.2 (red). Red arrowheads, transfected neurons; white arrowheads, untransfected neurons.

(D) Summary of the effects of Kv3 channel expression on endogenous Nav1.2 level at soma. 1, Kv3.1bHA (10); 2, Kv3.2b (9); 3, Kv3.3 (11); 4, Kv3.4aHA (10). One-way ANOVA followed by Dunnett's test: *$p < 0.05$.

(E–H) In old neurons (17 DIV), localization of expressed Kv3.1bHA (E), Kv3.2b (F), Kv3.3 (G), and Kv3.4aHA (H) versus endogenous pan-Nav channels was examined.

Despite the clear experimental results, our analyses only included a limited number of Nav and Kv channels. In mammalian genome, there are 14 genes for Nav α and β subunits and 12 subfamilies of Kv channel genes (total 40). Therefore, it remained unknown whether other potential players are involved in FS induction.

Genome-wide Analysis Reveals Robust Correlation of Kv3 and Nav mRNA Levels with FS

To unbiasedly determine all the potential key channel genes involved in FS induction, we performed RNA sequencing (RNA-seq)-based genome-wide analysis of correlations of mRNA levels of Nav and Kv channels with the firing frequency in different central neurons. The major assumption is that the total mRNA level of a

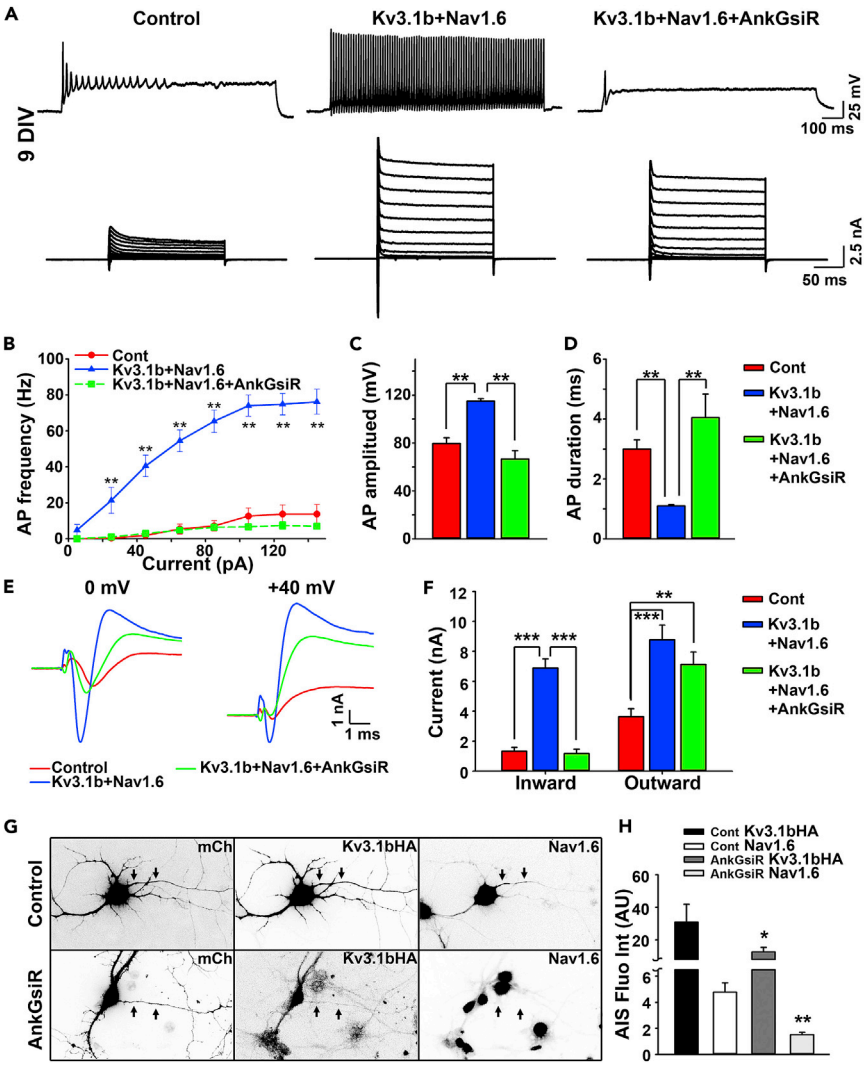

Figure 6. Knocking Down Ankyrin-G Significantly Altered the Balance of Nav and Kv3.1 Channels, Leading to Disrupted FS

(A) Example traces of current- (top) and voltage- (bottom) clamp recording of neurons transfected with YFP alone, Nav1.6 + Kv3.1b, or Nav1.6 + Kv3.1b + AnkGsiR.

(B) The input-output relationship.

(C) Summary of AP amplitude.

(D) Summary of AP duration.

(E) Extended current traces of voltage-clamp recording (the initial 6 ms) at the command potentials of 0 mV (left) and +40 mV (right).

(F) Summary of inward and outward currents under three different conditions.

(G) Localization of Nav1.6 and Kv3.1bHA in neurons with (top) and without (bottom) AnkGSiR.

(H) Summary of Nav1.6 and Kv3.1bHA staining intensities at the AIS.

Unpaired t test was used. *$p < 0.05$, **$p < 0.01$, ***$p < 0.001$.

gene generally correlates with its total protein level. RNA-seq datasets of 14 different types of neurons labeled by YFP under various promoters (*Ctgf*, *Ndnf*, *Rbp4*, *Chma2*, *Chat*, *Htr3a*, *Nr5a1*, *Sst*, *Scnn1a*, *Gad2*, *Vip*, and *Pavlb*) were obtained from the Allen Institute for Brain Science. The average maximal firing frequencies of these neurons are either available from the Allen Institute for Brain Science or from the literature. The neurons were divided into four groups based on the frequencies: high firing (*Pvalb* in the visual cortex; *Pvalb* in the auditory cortex and globus pallidus), medium high firing (*Gad2* in the lateral hypothalamus and visual cortex, *Sst* and *Scnn1a* in the visual cortex), medium firing (*Nr5a1* in the visual cortex, *Sst* in

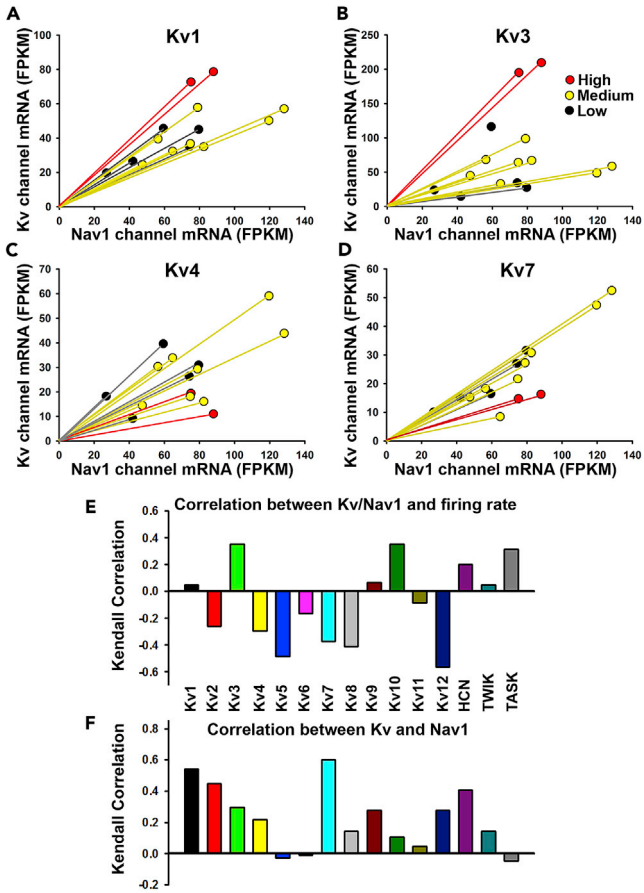

Figure 7. The mRNA Ratio between Kv3 and Nav1 Channels Best Correlates with the Firing Rate among all K^+ Channel Subfamilies

RNA-seq datasets were obtained from the Allen Institute for Brain Science.

(A) Correlation between Kv1 and Nav1 channels in 14 different types of neurons. The FPKM values of all the isoforms of Kv1 channel subfamily were added up with equal weight to represent the overall Kv1 channel expression. The Fragments Per Kilobase of transcript per Million mapped reads (FPKM) values of all the isoforms of Nav1 channels were added up to represent the overall Nav1 channel expression.

(B) Correlation between Kv3 and Nav1 channels. The FPKM values of all the isoforms (Kv3.1–Kv3.4) of Kv3 channel subfamily were added up to represent the overall Kv3 channel expression.

(C) Correlation between Kv4 and Nav1 channels.

(D) Correlation between Kv7 and Nav1 channels. High-firing neurons are shown in red, medium-firing neurons in yellow, and low-firing neurons in black.

(E) Correlations between the K^+/Nav1 ratio and the firing rate in different neurons.

(F) Correlations between the K^+ channel subfamilies and Nav1 channels in different neurons, regardless of the firing rate. In (E) and (F), each color indicates a channel subfamily.

the auditory cortex, and *Htr3a* in the anterior lateral motor area), and low firing (*Chat*, *Chrna2*, *Ctgf*, *Ndnf*, and *Rbp4* in the visual cortex) (Hilscher et al., 2017; Karnani et al., 2013; Lee et al., 2010; Levy and Reyes, 2012; Mastro et al., 2014; Sotty et al., 2003; Tyan et al., 2014).

First, we determined the correlations between different Kv channel subfamilies and Nav pore-forming α-subunit (Nav1) family. Due to their implicated roles in FS, HCN and two-pore K^+ channel subfamilies (TWIK and TASK) were also included in the analysis. The mRNA counts of different channel isoforms within the same subfamily were added together with equal weight. This is because our experimental results suggest that different isoforms of Kv3 and Nav channels appear interchangeable (Figures 1, 3 and 4). We generated one graph for each pair of Kv channel subfamily and Nav1 channel and grouped the neurons with medium high and medium firing rates into one group here. Kv3 channel subfamily clearly stood out for the strongest apparent correlation of Kv3/Nav1 ratio and firing rate (Figures 7A–7D and S4). In sharp contrast, the ratios of Kv4 and Kv7 inversely

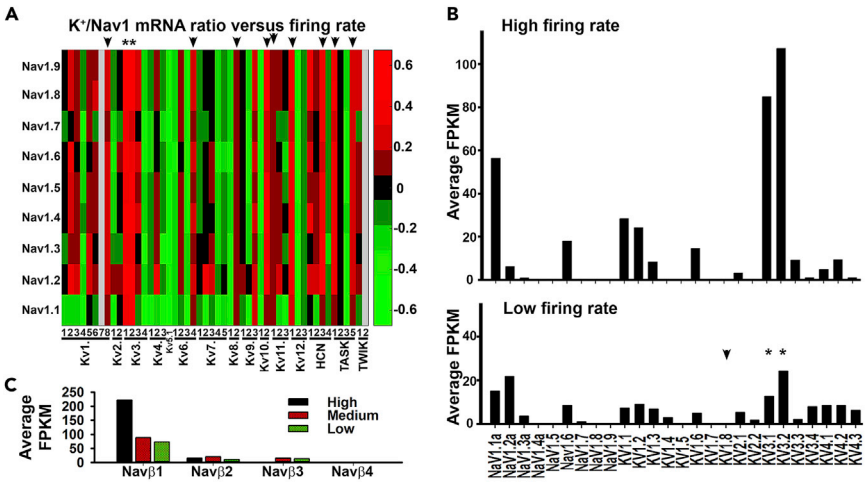

Figure 8. Correlation of the Ratio between Individual K^+ and Nav1 Channels with the Firing Frequency

RNA-seq datasets were obtained from the Allen Institute for Brain Science.

(A) The heatmap shows correlation of the ratios between individual K^+ and Nav1 channels with the firing frequency. Positive correlations are shown in red, whereas negative correlations are shown in green. Two best correlations, Kv3.1 and Kv3.2, are indicated with "*." The second-tier genes of good correlations are indicated with black arrowheads.

(B) mRNA levels of individual Nav1 and Kv(1–4) channels in neurons with high (top) and low (bottom) firing rate.

(C) mRNA levels of Navβ subunits, including Navβ4, in neurons with high, medium and low firing rates.

correlated with the firing rate (Figures 7C and 7D). Interestingly, the ratios of Kv1 or Kv7 mRNA and Nav1 mRNA fall into a very narrow range in all the neurons regardless of the firing rate (Figures 7A and 7D).

Next, we performed Kendall correlation (Kendall, 1938) between the channel mRNA ratio and the firing rate (four groups here: high, medium high, medium, and low firing). Kv3, Kv10, and TASK subfamilies were the top three with positive correlation, indicating that the high ratio between their mRNA and Nav1 mRNA is associated with a high firing rate in neurons (Figure 7E). In contrast, Kv12, Kv5, Kv8, and Kv7 were the top four negative correlations, indicating that the high ratio between their mRNA and Nav1 mRNA is associated with a low firing rate in neurons (Figure 7E). Furthermore, it is important to note that the total mRNA level of Kv3 (up to ~220) was approximately 36-and 12-fold higher than those of Kv10 (up to ~6) and TASK (up to ~18), respectively (Figures 7B, S4F, and S4K). It is most likely that such a major difference at the mRNA level reflects a substantial difference at the protein level as well. Therefore, Kv3 is the only Kv subfamily whose ratio with Nav1 channels well correlates with the firing frequency in neurons.

In Kendall correlation between Kv and Nav1 channel subfamilies in all neurons regardless of the firing rate, Kv7, Kv1, and Kv2 subfamilies were the top three (Figure 7F). This result suggests that these Kv channels are important balancers (providing outward currents) to Nav1 channels (providing inward currents) to ensure AP firing in all neurons.

Finally, we performed Kendall correlation between the mRNA ratio of individual channel genes and the firing rate (four groups here: high, medium high, medium, and low firing). The most correlated genes were Kv3.1 and Kv3.2, correlating extremely well with all Nav1 isoforms (Figure 8A). The second tier group of correlative genes included Kv1.8, Kv6.4, Kv8.2, Kv10.2, Kv11.1, Kv12.1, HCN3, TASK1, and TASK5 (Figure 8A). However, these second tier genes all had much lower mRNA levels compared with those of Kv3.1 and Kv3.2 (Figures 8B and S5) and hence are unlikely to play an important role in FS induction and maintenance. Furthermore, we examined Navβ subunits, from Navβ1 to Navβ4, in all neurons that were grouped into high, medium, and low firing. The mRNA levels of Navβ4 were insignificant compared with those of other Navβ genes (Figure 8C), arguing against a major role played by Navβ4 in FS induction in all central neurons.

DISCUSSION

Our results have demonstrated that activities of both Kv3 and Nav channels are required for FS induction and maintenance. When being activated in a proper ratio, the two are sufficient to induce FS, which

appears to be true for all isoforms of Kv3 and Nav channels (Figure S6). This is the foundational condition that is sufficient and necessary for inducing FS that is defined by high firing frequency, uniform AP amplitude, and interspike intervals (Figure S6). The maximal frequency of FS can be further adjusted by secondary factors, including the quantitative differences in biophysical properties of channel isoforms within the subfamily, membrane targeting patterns of the channel proteins, significant expression of other types of ion channels, post-translational modifications, and transcriptional and translational modifications (Figure S6).

Kv3 Channels Are Necessary but Not Sufficient for FS Induction in Mammalian Central Neurons

The overall biophysical properties of Kv3 channel isoforms are similar in terms of high activation threshold and rapid activation and deactivation kinetics. However, these parameters quantitatively differ for different Kv3 isoforms. Which biophysical parameter is the most important one for FS induction and maintenance? To answer this question, we analyzed the four Kv3 constructs expressed in HEK293 cells: Kv3.1b, Kv3.2b, Kv3.3, and Kv3.4a, which is a thorough representation of all the members of the Kv3 subfamily, since alternative splicing at the C terminus does not affect the channel biophysical properties. All fourKv3 isoforms had high activation threshold (>−20 mV) (Figure 2D), suggesting its importance. This is because all Kv3 channels appeared capable of supporting FS in mature neurons (Figures 1D and S1). In sharp contrast, inactivation observed for Kv3.3 and Kv3.4a appeared to play no role in FS, potentially due to its long timescale (>100 ms) (Figure 2A). Furthermore, Kv3.2 and Kv3.3 had relatively slower activation compared with Kv3.1b and Kv3.4; Kv3.2 and Kv3.4 had relatively slower deactivation compared with Kv3.1b and Kv3.3 (Figures 2E and 2F). However, compared with Kv1.2 (τ_{on}: ~ 2.5 ms; τ_{off}: ~ 3.0 ms) and other slower Kv channels, these values for all Kv3 channels appear to be sufficient for FS induction.

Different from the other three Kv3 constructs, Kv3.2b displayed a large range in its activation time constant but not its deactivation time constant (Figures 2G and 2H). Its activation in some transfected HEK293 cells was as rapid as that of Kv3.1b, but similar to that of Kv1.2 in other transfected HEK293 cells (Figure 2G). Surprisingly, Kv3.2b was as effective as Kv3.1b in converting SS neurons to FS (Figures 1 and S1). It is possible that an endogenous factor that is present in hippocampal neurons but not in HEK293 cells regulates Kv3.2 activation kinetics. It will be interesting to further determine whether this factor also plays a role in regulating AP firing in Kv3.2-expressing SST+ GABAergic interneurons, which normally do not display FS. This is an interesting topic for future investigation. Despite the interesting findings, the analysis of channel biophysical properties did not enable us to isolate one parameter key to FS and to explain why Kv3.3 expression did not induce FS in young neurons.

Interestingly, the role of Kv3 channels in FS appears not evolutionarily conserved. Mammalian Kv3 channels are orthologs of the Shaw channel in fruit fly *Drosophila* (Haas et al., 1993). The Shaw channel activates at more negative potentials and in slower kinetics compared with the Kv3 channels (Wei et al., 1990). It was speculated that the conservation of this channel family through evolution may reflect some aspect of channel function other than K^+ influx, perhaps protein-protein interactions with other cellular components (Kaczmarek, 2006; Kaczmarek and Zhang, 2017). It currently remains unclear whether and how invertebrate animals utilize FS neurons in their nervous systems to carry out important neurophysiological functions. Therefore, the present study only draws conclusions for the mammalian nervous systems.

Trafficking of Kv3 and Nav Channels Plays a Regulatory Role in FS

When expressed in HEK293 cells, Kv3.3 displayed slower activation than Kv3.1b, but it was comparable to that of Kv3.2b (Figure 2). Kv3.3 also had inactivation similar to Kv3.4a (Figure 2). Thus, the inability of Kv3.3 in FS induction in young neurons is unlikely due to its biophysical properties. Interestingly, our staining results reveal that the expression of Kv3.3 but not the other three types of Kv3 constructs markedly reduced the endogenous Nav1.2 channel level at the soma of young neurons (Figure 5). In contrast, none of the Kv3 constructs affected Nav channel overall levels or its level at the AIS in mature neurons (Figure 5). This appears consistent with the voltage-clamp results of transfected neurons in the amplitude of their inward currents (Figure 3). Why did Kv3.3 expression affect Nav channel levels in young neurons but not in older neurons? It is possible that Kv3.3 channel proteins compete with Nav channel proteins for trafficking machinery in young neurons. Our previous studies showed that Kv3.1b channel directly binds to conventional kinesin KIF5B and AnkG via conserved regions in its N and C termini, respectively

(Xu et al., 2007, 2010). Due to the presence of these conserved regions in Kv3.3, Kv3.3 likely binds to KIF5B and AnkG as well. Our recent studies showed that KIF5B and AnkG are critical for Nav1.2 axonal transport, as well as for its general forward trafficking (Barry et al., 2014), raising the possibility of competing trafficking between Kv3.3 and Nav1.2. Furthermore, a recent study reported that Kv3.3 channels are specifically linked to actin cytoskeleton via HS-1 associated protein X-1 (Hax-1), an anti-apoptotic protein that regulates actin nucleation through Arp2/3 (Zhang et al., 2016). Hax-1 and cortical actin network regulate the membrane localization and inactivation of Kv3.3 channels (Zhang et al., 2016). The Kv3.3-Hax-1 binding is mediated by a non-conserved proline-rich region in the cytoplasmic C terminus of Kv3.3 channel (Zhang et al., 2016). These findings provide important clues for understanding how Kv3.3 exactly competes with Nav channels in young neurons in future studies. On the other hand, mature (or older) neurons (at 15 DIV) likely already have enough endogenous Nav channel proteins at the right places, including the AIS. So endogenous Nav channels are less likely altered by Kv3.3 channel transient expression in mature neurons.

All Nav1 Channel Isoforms Expressed in the CNS Should Be Capable of Supporting FS

Our results indicate that a proper balance of Kv3 and Nav channels is critical for FS (Figures 3 and 4). Consistent with this notion, large Kv3 but small Nav currents are unlikely able to support FS. One extreme example is starburst amacrine cells. They are the only retinal neurons containing acetylcholine and can generate spiking-like potentials. Although it was debated whether amacrine cells can generate real APs (Cohen, 2001), they are certainly unable to display FS. Interestingly, in starburst amacrine cells in mouse retina, large Kv3 currents (up to 10 nA) were detected to be mainly carried by Kv3.1 and Kv3.2 channels (Ozaita et al., 2004), whereas the average Nav current was very small, around 0.12 nA (Cohen, 2001). Their inability of FS is consistent with our model.

In the present study, we provide several lines of evidence to support our new model that a proper balance of Kv3 and Nav channel activities is necessary and sufficient for FS induction. First, our analysis of SS and FS neurons that were transfected revealed that high inward (Nav) currents are critical for FS young neurons, whereas high outward (Kv) currents are critical for FS old neurons (Figures 3 and S2). As discussed in the previous section, endogenous Nav1 channels are normally low at the early developmental stage and more likely to be disrupted by Kv3 channel expression. It is possible that only those young neurons with sufficient amount of Nav channel proteins can be converted into FS. In sharp contrast, endogenous Nav channel proteins in mature neurons are less likely disrupted by Kv3 expression, when Kv3 expression level becomes a determinant due to potential interference by high levels of other types of endogenous ion channels.

Second, co-expression of Kv3 and Nav1 channels resulted in FS with 100% efficiency (Figures 4 and S3). In fact, the maximal firing frequencies of any combination between Nav1.2/Nav1.6 and Kv3.1/Kv3.3 were similar (Figure 4), although these channels have different biophysical properties. It is important to note that increasing the Nav1 expression alone (including Nav1.6) did not increase the firing frequency at all (Figure 4). Moreover, our results indicated that Nav1.2, as well as Nav1.6, can operate together with Kv3 channels to support FS. Nav1.6 but not Nav1.2 was implicated in resurgent Na^+ currents (Cummins et al., 2005; Lewis and Raman, 2014; Raman et al., 1997). Third, our analysis with the RNA-seq data shows a robust correlation between Kv3/Nav1 mRNA ratio and firing frequency (Figures 7, 8, and S5). It is important to note that the level of Nav1.1 is the highest in PV+ FS interneurons and correlates well with the firing rate of the neurons (Figures 8 and S5). It strongly suggests that Nav1.1 can support FS as well if co-expressed with Kv3 channels. Therefore, FS induction does not seem limited only to a few isoforms of Kv3 and Nav1 channel families; instead it appears that all isoforms in these two families are capable of supporting FS.

Resurgent Nav channels may not be necessary and are certainly not sufficient for FS induction. Nav1.1, Nav1.2, and Nav1.6 are the three major neuronal Nav1 channels, and all can support FS. Together with YFP-Kv1.2, Nav1.6 appeared slightly more effective than Nav1.2 in increasing the AP firing frequency (Figure 4). However, the AP firing pattern with Nav1.6 and YFP-Kv1.2 is still different from FS. Among all non-Kv3 isoforms, Kv1.2 is the fastest in terms of activation and deactivation kinetics. On the other hand, the mRNA levels of Navβ4 are very low compared with other Navβ subunits based on our analysis with RNA-seq databases (Figure 8C). Therefore, Nav1.6 and Navβ4 are unlikely to play a primary role in FS induction. It is important to note that we mainly focus on the maximal firing frequency of FS neurons in the present

study. There are certainly other means to alter the firing frequencies of other types of neurons, for instance, SS neurons.

Potential Regulatory Roles of Other Types of Ion Channels in FS

Although we show that Kv3 (Kv3.1b and Kv3.3) and Nav1 (Nav1.2 and Nav1.6) together are capable of inducing FS in SS hippocampal neurons (Figure 4), it was still unknown whether FS neurons indeed use these native channels for their AP firing *in vivo*, and whether other unexpected channels are involved in FS induction. To address these questions, we performed a genome-wide analysis using RNA-seq database available from the Allen Institute for Brain Science, by focusing on all Nav and Kv channels, as well as the channels that were implicated in FS neuron functions, including HCN and two-pore K^+ channels (Figures 7, 8, S4, and S5). This represents the first attempt of using genome-wide analysis to address this question in the field, thanks to the availability of the database from the Allen Institute for Brain Science. Each type of neurons expresses a distinct set of ion channels at different levels, and the neuronal excitability features reflect a compromise of channel actions. Kv3 channel subfamily is the best in terms of its ratio to Nav1 channels correlating with neuronal firing rates in different neurons (Figures 7 and S4). The only outlier of Kv3/Nav1 ratio and firing rate is the *Chat* neuron, which is low-firing-frequency neuron, although both its Kv3/Nav1 ratio and Kv3 mRNA level are reasonably high (Figure 7B). However, after examining the expression of individual genes, we found that Kv3.2 but not Kv3.1 channel mRNA is the predominant species within the Kv3 subfamily expressed in the *Chat* neuron. Given its unique biophysical feature in activation kinetics (Figure 2), Kv3.2 may activate very slowly to support FS in some central neurons due to the lack of that endogenous modulator, such as the *Chat* neurons. Among individual Kv3 channels, Kv3.3 and Kv3.4 mRNAs do not appear to correlate with FS in central neurons (Figures 8 and S5).

Kv10 and TASK channels were ranked the second and third in such correlation, behind Kv3 channels (Figure 7E). However, the absolute levels of Kv10 and TASK are too low to be a major player in influencing the firing rate (Figures 8 and S5). Importantly, their activation and deactivation kinetics are also significantly slower than those of Kv3 channels. Thus, they are unlikely to be a determinant for FS induction. In contrast, it appears that the high expression levels of Kv4 and Kv7 (as well as Kv5 and Kv12) appear to negatively correlate with FS neurons (Figures 7C–7E). The significant presence of these Kv channels with slow activation kinetics likely reduces the intrinsic firing rate of the neurons.

Our analysis has revealed another interesting point that the level of Kv1, Kv2, or Kv7 strongly correlates with the level of Nav1 channels in all neurons examined, regardless of their firing rates (Figures 7A, 7D, 7F, and S4). This result suggests that these channels play a key role in maintaining the balance of inward and outward currents in various neurons to ensure the generation of APs in general. This appears consistent with the functions of these channels. Taken together, the genome-wide analysis not only provided strong support to our model based on our electrophysiological data but also revealed interesting unexpected points that will be further evaluated in future investigation.

Alteration of FS through Regulation of Kv3 and Nav Channels in Health and Disease

Mutations of Nav1 and Kv3 channels have been identified and linked to diseases in humans. Mutations in the Nav1.1 (SCN1A) channel are responsible for a number of epilepsies, from mild early-life febrile seizures to Dravet syndrome (severe myoclonic epilepsy of infancy) (Genton et al., 2011; Li et al., 2011; Wolff et al., 2006). However, it is interesting that, among hundreds of identified Nav1.1 mutations, both decreasing and increasing channel activity can cause hyper-excitability of neural networks and hence epileptic seizures (Ragsdale, 2008). Based on our new model, Nav1.1 mutations may alter the proper ratio between Kv3 and Nav1 channels, and hence disrupt neuronal AP firing. Indeed, both Nav1.1 and Kv3.1 channels are expressed in PV+ interneurons (Hu et al., 2014; Ogiwara et al., 2007), and their imbalanced activities may reduce interneuron firing leading to hyper-excitability of neural networks. Mutations in Nav1.2 and Nav1.6 were found to associate with epilepsies and neurodevelopmental disorders (O'Brien, 2013; Wolff et al., 2017). On the other hand, mutations in Kv3.1 and Kv3.3 genes reportedly lead to progressive myoclonic epilepsy and spinocerebellar ataxia, respectively (Figueroa et al., 2010; Muona et al., 2015; Waters et al., 2006). Our new model may help to gain new mechanistic insights into the pathogenesis of these disorders.

Regulations of individual Kv3 and Nav1 channels have been extensively studied, especially the regulation at the level of post-translational modification (i.e., protein phosphorylation) (for details see reviews Catterall,

2012; Kaczmarek and Zhang, 2017). To study one channel at a time has been a major research strategy in the field. Our new model indicates that the regulation of AP firing patterns may be better understood through examining the balance of Na^+ and K^+ channels.

Limitations of the Study

In the present study, we only measured AP firing using a recording pipette from the neuronal soma, picking up the back-propagating AP from the AIS, where APs are initiated. The polarized axon-dendrite targeting of Kv3 channels may certainly affect neuronal electrical signaling, especially in distal processes including axonal terminals and distal dendrites. It will be an interesting topic for future investigation. Of note, the values of inward (I_{in}) and outward (I_{out}) currents may not accurately represent the Nav and Kv currents in the neuron due to potential space-clamp problem, large Nav currents not being completely clamped, and incomplete temporal segregation of the two currents. Nonetheless, these values of I_{in} and I_{out} are well defined here, allowing us to perform current-clamp and voltage-clamp recordings on the same neuron under the same condition. With this caveat, we cautiously interpreted our results in this study.

Why did Kv3.3 expression affect Nav channel levels in young neurons? Although we have discussed the possibility that Kv3.3 channel proteins compete with Nav channel proteins for trafficking machinery in young neurons in a previous section, we currently do not have any additional experimental data to address this question. Moreover, an unknown regulatory factor may be involved to complicate the problem. This represents a question that has been raised by this study for future investigation.

It is important to note that the mRNA level may not always perfectly correlate with the protein level for any particular gene that expresses in a neuron. Furthermore, even the total protein level of an ion channel may not perfectly correlate with its level on the neuronal surface, which is a prerequisite for the channel's role in AP firing. While keeping these caveats in mind, we assumed that mRNA levels overall correlate with protein levels for most genes. Moreover, this is the best database that is currently available for our analysis.

METHODS

All methods can be found in the accompanying Transparent Methods supplemental file.

SUPPLEMENTAL INFORMATION

Supplemental Information includes Transparent Methods, six figures, and one table and can be found with this article online at https://doi.org/10.1016/j.isci.2018.10.014.

ACKNOWLEDGMENTS

We thank Drs. Alan Golding, Theodore R. Cummins, and Tatiana Tkatch for cDNA constructs, and Dr. Leonard Kaczmarek for comments on the manuscript. This work was supported, in part, by grants from the US National Institute of Neurological Disorders and Stroke/National Institutes of Health (R01NS062720 and R01NS093073 to C.G. and R01NS091144 to J.B.D), the National Natural Science Foundation of China (61572265 to Z.H.), and the Shenzhen Peacock Plan (KQTD2016053112051497 to K.H). All animal experiments have been conducted in accordance with the NIH Animal Use Guidelines.

AUTHOR CONTRIBUTIONS

C.G. designed and supervised the research. Y.G., R.L.L, J.B.D., and C.G. performed experiments, analyzed data, and made figures. D.S., Z.H., and K.H. performed the bioinformatics analysis. C.G. wrote the paper. All the authors participated in revising the manuscript.

DECLARATION OF INTERESTS

The authors declare no competing interests.

Received: May 1, 2018
Revised: August 11, 2018
Accepted: October 12, 2018
Published: November 30, 2018

REFERENCES

Aponte, Y., Lien, C.C., Reisinger, E., and Jonas, P. (2006). Hyperpolarization-activated cation channels in fast-spiking interneurons of rat hippocampus. J. Physiol. *574*, 229–243.

Bant, J.S., and Raman, I.M. (2010). Control of transient, resurgent, and persistent current by open-channel block by Na channel beta4 in cultured cerebellar granule neurons. Proc. Natl. Acad. Sci. U S A *107*, 12357–12362.

Barry, J., Gu, Y., Jukkola, P., O'Neill, B., Gu, H., Mohler, P.J., Rajamani, K.T., and Gu, C. (2014). Ankyrin-G directly binds to kinesin-1 to transport voltage-gated Na+ channels into axons. Dev. Cell *28*, 117–131.

Barry, J., Xu, M., Gu, Y., Dangel, A.W., Jukkola, P., Shrestha, C., and Gu, C. (2013). Activation of conventional kinesin motors in clusters by Shaw voltage-gated K+ channels. J. Cell Sci. *126*, 2027–2041.

Bean, B.P. (2007). The action potential in mammalian central neurons. Nat. Rev. Neurosci. *8*, 451–465.

Biel, M., Wahl-Schott, C., Michalakis, S., and Zong, X. (2009). Hyperpolarization-activated cation channels: from genes to function. Physiol. Rev. *89*, 847–885.

Catterall, W. (2012). Voltage-gated sodium channels at 60: structure, function and pathophysiology. J. Physiol. *590*, 2577–2589.

Catterall, W.A., Kalume, F., and Oakley, J.C. (2010). NaV1.1 channels and epilepsy. J. Physiol. *588*, 1849–1859.

Chow, A., Erisir, A., Farb, C., Nadal, M.S., Ozaita, A., Lau, D., Welker, E., and Rudy, B. (1999). K(+) channel expression distinguishes subpopulations of parvalbumin- and somatostatin-containing neocortical interneurons. J. Neurosci. *19*, 9332–9345.

Cohen, E.D. (2001). Voltage-gated calcium and sodium currents of starburst amacrine cells in the rabbit retina. Vis. Neurosci. *18*, 799–809.

Cummins, T.R., Dib-Hajj, S.D., Herzog, R.I., and Waxman, S.G. (2005). Nav1.6 channels generate resurgent sodium currents in spinal sensory neurons. FEBS Lett. *579*, 2166–2170.

Diwakar, S., Magistretti, J., Goldfarb, M., Naldi, G., and D'Angelo, E. (2009). Axonal Na+ channels ensure fast spike activation and back-propagation in cerebellar granule cells. J. Neurophysiol. *101*, 519–532.

Du, J., Zhang, L., Weiser, M., Rudy, B., and McBain, C.J. (1996). Developmental expression and functional characterization of the potassium-channel subunit Kv3.1b in parvalbumin-containing interneurons of the rat hippocampus. J. Neurosci. *16*, 506–518.

Enomoto, A., Han, J.M., Hsiao, C.F., Wu, N., and Chandler, S.H. (2006). Participation of sodium currents in burst generation and control of membrane excitability in mesencephalic trigeminal neurons. J. Neurosci. *26*, 3412–3422.

Erisir, A., Lau, D., Rudy, B., and Leonard, C.S. (1999). Function of specific K(+) channels in sustained high-frequency firing of fast-spiking neocortical interneurons. J. Neurophysiol. *82*, 2476–2489.

Espinosa, F., Marks, G., Heintz, N., and Joho, R.H. (2004). Increased motor drive and sleep loss in mice lacking Kv3-type potassium channels. Genes Brain Behav. *3*, 90–100.

Figueroa, K.P., Minassian, N.A., Stevanin, G., Waters, M., Garibyan, V., Forlani, S., Strzelczyk, A., Burk, K., Brice, A., Durr, A., et al. (2010). KCNC3: phenotype, mutations, channel biophysics-a study of 260 familial ataxia patients. Hum. Mutat. *31*, 191–196.

Genton, P., Velizarova, R., and Dravet, C. (2011). Dravet syndrome: the long-term outcome. Epilepsia *52* (*Suppl 2*), 44–49.

Gittis, A.H., and du Lac, S. (2006). Intrinsic and synaptic plasticity in the vestibular system. Curr. Opin. Neurobiol. *16*, 385–390.

Gu, C., and Barry, J. (2011). Function and mechanism of axonal targeting of voltage-sensitive potassium channels. Prog. Neurobiol. *94*, 115–132.

Gu, Y., Barry, J., McDougel, R., Terman, D., and Gu, C. (2012). Alternative splicing regulates kv3.1 polarized targeting to adjust maximal spiking frequency. J. Biol. Chem. *287*, 1755–1769.

Haas, M., Ward, D.C., Lee, J., Roses, A.D., Clarke, V., D'Eustachio, P., Lau, D., Vega-Saenz de Miera, E., and Rudy, B. (1993). Localization of Shaw-related K+ channel genes on mouse and human chromosomes. Mamm. Genome *4*, 711–715.

Hilscher, M.M., Leao, R.N., Edwards, S.J., Leao, K.E., and Kullander, K. (2017). Chrna2-martinotti cells synchronize layer 5 type A pyramidal cells via rebound excitation. PLoS Biol. *15*, e2001392.

Hu, H., Gan, J., and Jonas, P. (2014). Interneurons. fast-spiking, parvalbumin+ GABAergic interneurons: from cellular design to microcircuit function. Science *345*, 1255263.

Hughes, D.I., Boyle, K.A., Kinnon, C.M., Bilsland, C., Quayle, J.A., Callister, R.J., and Graham, B.A. (2013). HCN4 subunit expression in fast-spiking interneurons of the rat spinal cord and hippocampus. Neuroscience *237*, 7–18.

Hughes, D.I., Sikander, S., Kinnon, C.M., Boyle, K.A., Watanabe, M., Callister, R.J., and Graham, B.A. (2012). Morphological, neurochemical and electrophysiological features of parvalbumin-expressing cells: a likely source of axo-axonic inputs in the mouse spinal dorsal horn. J. Physiol. *590*, 3927–3951.

Hurlock, E.C., Bose, M., Pierce, G., and Joho, R.H. (2009). Rescue of motor coordination by Purkinje cell-targeted restoration of Kv3.3 channels in Kcnc3-null mice requires Kcnc1. J. Neurosci. *29*, 15735–15744.

Joho, R.H., Ho, C.S., and Marks, G.A. (1999). Increased gamma- and decreased delta-oscillations in a mouse deficient for a potassium channel expressed in fast-spiking interneurons. J. Neurophysiol. *82*, 1855–1864.

Kaczmarek, L.K. (2006). Non-conducting functions of voltage-gated ion channels. Nat. Rev. Neurosci. *7*, 761–771.

Kaczmarek, L.K., and Zhang, Y. (2017). Kv3 channels: enablers of rapid firing, neurotransmitter release, and neuronal endurance. Physiol. Rev. *97*, 1431–1468.

Karnani, M.M., Szabo, G., Erdelyi, F., and Burdakov, D. (2013). Lateral hypothalamic GAD65 neurons are spontaneously firing and distinct from orexin- and melanin-concentrating hormone neurons. J. Physiol. *591*, 933–953.

Kendall, M. (1938). A new measure of rank correlation. Biometrika *30*, 81–93.

Kuba, H., Ishii, T.M., and Ohmori, H. (2006). Axonal site of spike initiation enhances auditory coincidence detection. Nature *444*, 1069–1072.

Kuba, H., Oichi, Y., and Ohmori, H. (2010). Presynaptic activity regulates Na(+) channel distribution at the axon initial segment. Nature *465*, 1075–1078.

Labro, A.J., Priest, M.F., Lacroix, J.J., Snyders, D.J., and Bezanilla, F. (2015). Kv3.1 uses a timely resurgent K(+) current to secure action potential repolarization. Nat. Commun. *6*, 10173.

Lee, S., Hjerling-Leffler, J., Zagha, E., Fishell, G., and Rudy, B. (2010). The largest group of superficial neocortical GABAergic interneurons expresses ionotropic serotonin receptors. J. Neurosci. *30*, 16796–16808.

Levy, R.B., and Reyes, A.D. (2012). Spatial profile of excitatory and inhibitory synaptic connectivity in mouse primary auditory cortex. J. Neurosci. *32*, 5609–5619.

Lewis, A.H., and Raman, I.M. (2014). Resurgent current of voltage-gated Na(+) channels. J. Physiol. *592*, 4825–4838.

Lewis, D.A., Hashimoto, T., and Volk, D.W. (2005). Cortical inhibitory neurons and schizophrenia. Nat. Rev. Neurosci. *6*, 312–324.

Li, B.M., Liu, X.R., Yi, Y.H., Deng, Y.H., Su, T., Zou, X., and Liao, W.P. (2011). Autism in Dravet syndrome: prevalence, features, and relationship to the clinical characteristics of epilepsy and mental retardation. Epilepsy Behav. *21*, 291–295.

Lien, C.C., and Jonas, P. (2003). Kv3 potassium conductance is necessary and kinetically optimized for high-frequency action potential generation in hippocampal interneurons. J. Neurosci. *23*, 2058–2068.

Magistretti, J., Castelli, L., Forti, L., and D'Angelo, E. (2006). Kinetic and functional analysis of transient, persistent and resurgent sodium currents in rat cerebellar granule cells in situ: an electrophysiological and modelling study. J. Physiol. *573*, 83–106.

Marin, O. (2012). Interneuron dysfunction in psychiatric disorders. Nat. Rev. Neurosci. *13*, 107–120.

Martina, M., Metz, A.E., and Bean, B.P. (2007). Voltage-dependent potassium currents during fast spikes of rat cerebellar Purkinje neurons:

inhibition by BDS-I toxin. J. Neurophysiol. *97*, 563–571.

Mastro, K.J., Bouchard, R.S., Holt, H.A., and Gittis, A.H. (2014). Transgenic mouse lines subdivide external segment of the globus pallidus (GPe) neurons and reveal distinct GPe output pathways. J. Neurosci. *34*, 2087–2099.

McCormick, D.A., Connors, B.W., Lighthall, J.W., and Prince, D.A. (1985). Comparative electrophysiology of pyramidal and sparsely spiny stellate neurons of the neocortex. J. Neurophysiol. *54*, 782–806.

Muona, M., Berkovic, S.F., Dibbens, L.M., Oliver, K.L., Maljevic, S., Bayly, M.A., Joensuu, T., Canafoglia, L., Franceschetti, S., Michelucci, R., et al. (2015). A recurrent de novo mutation in KCNC1 causes progressive myoclonus epilepsy. Nat. Genet. *47*, 39–46.

Nakazawa, K., Zsiros, V., Jiang, Z., Nakao, K., Kolata, S., Zhang, S., and Belforte, J.E. (2012). GABAergic interneuron origin of schizophrenia pathophysiology. Neuropharmacology *62*, 1574–1583.

O'Brien, M. (2013). Sodium channel SCN8A (Nav1.6): properties and de novo mutations in epileptic encephalopathy and intellectual disability. Front. Genet. *4*, 213.

Ogiwara, I., Miyamoto, H., Morita, N., Atapour, N., Mazaki, E., Inoue, I., Takeuchi, T., Itohara, S., Yanagawa, Y., Obata, K., et al. (2007). Nav1.1 localizes to axons of parvalbumin-positive inhibitory interneurons: a circuit basis for epileptic seizures in mice carrying an Scn1a gene mutation. J. Neurosci. *27*, 5903–5914.

Okaty, B.W., Miller, M.N., Sugino, K., Hempel, C.M., and Nelson, S.B. (2009). Transcriptional and electrophysiological maturation of neocortical fast-spiking GABAergic interneurons. J. Neurosci. *29*, 7040–7052.

Ozaita, A., Martone, M.E., Ellisman, M.H., and Rudy, B. (2002). Differential subcellular localization of the two alternatively spliced isoforms of the Kv3.1 potassium channel subunit in brain. J. Neurophysiol. *88*, 394–408.

Ozaita, A., Petit-Jacques, J., Volgyi, B., Ho, C.S., Joho, R.H., Bloomfield, S.A., and Rudy, B. (2004). A unique role for Kv3 voltage-gated potassium channels in starburst amacrine cell signaling in mouse retina. J. Neurosci. *24*, 7335–7343.

Ragsdale, D.S. (2008). How do mutant Nav1.1 sodium channels cause epilepsy? Brain Res. Rev. *58*, 149–159.

Raman, I.M., and Bean, B.P. (1997). Resurgent sodium current and action potential formation in dissociated cerebellar Purkinje neurons. J. Neurosci. *17*, 4517–4526.

Raman, I.M., Sprunger, L.K., Meisler, M.H., and Bean, B.P. (1997). Altered subthreshold sodium currents and disrupted firing patterns in Purkinje neurons of Scn8a mutant mice. Neuron *19*, 881–891.

Ransdell, J.L., Dranoff, E., Lau, B., Lo, W.L., Donermeyer, D.L., Allen, P.M., and Nerbonne, J.M. (2017). Loss of Navbeta4-mediated regulation of sodium currents in adult Purkinje neurons disrupts firing and impairs motor coordination and balance. Cell Rep. *19*, 532–544.

Rudy, B., Chow, A., Lau, D., Amarillo, Y., Ozaita, A., Saganich, M., Moreno, H., Nadal, M.S., Hernandez-Pineda, R., Hernandez-Cruz, A., et al. (1999). Contributions of Kv3 channels to neuronal excitability. Ann. N. Y Acad. Sci. *868*, 304–343.

Rudy, B., and McBain, C.J. (2001). Kv3 channels: voltage-gated K+ channels designed for high-frequency repetitive firing. Trends Neurosci. *24*, 517–526.

Sekirnjak, C., Martone, M.E., Weiser, M., Deerinck, T., Bueno, E., Rudy, B., and Ellisman, M. (1997). Subcellular localization of the K+ channel subunit Kv3.1b in selected rat CNS neurons. Brain Res. *766*, 173–187.

Song, P., Yang, Y., Barnes-Davies, M., Bhattacharjee, A., Hamann, M., Forsythe, I.D., Oliver, D.L., and Kaczmarek, L.K. (2005). Acoustic environment determines phosphorylation state of the Kv3.1 potassium channel in auditory neurons. Nat. Neurosci. *8*, 1335–1342.

Sotty, F., Danik, M., Manseau, F., Laplante, F., Quirion, R., and Williams, S. (2003). Distinct electrophysiological properties of glutamatergic, cholinergic and GABAergic rat septohippocampal neurons: novel implications for hippocampal rhythmicity. J. Physiol. *551*, 927–943.

Trimmer, J.S., and Rhodes, K.J. (2004). Localization of voltage-gated ion channels in mammalian brain. Annu. Rev. Physiol. *66*, 477–519.

Tyan, L., Chamberland, S., Magnin, E., Camire, O., Francavilla, R., David, L.S., Deisseroth, K., and Topolnik, L. (2014). Dendritic inhibition provided by interneuron-specific cells controls the firing rate and timing of the hippocampal feedback inhibitory circuitry. J. Neurosci. *34*, 4534–4547.

Vacher, H., Mohapatra, D.P., and Trimmer, J.S. (2008). Localization and targeting of voltage-dependent ion channels in mammalian central neurons. Physiol. Rev. *88*, 1407–1447.

Vonderschen, K., and Wagner, H. (2014). Detecting interaural time differences and remodeling their representation. Trends Neurosci. *37*, 289–300.

Wang, L.Y., Gan, L., Forsythe, I.D., and Kaczmarek, L.K. (1998). Contribution of the Kv3.1 potassium channel to high-frequency firing in mouse auditory neurones. J. Physiol. *509* (Pt 1), 183–194.

Waters, M.F., Minassian, N.A., Stevanin, G., Figueroa, K.P., Bannister, J.P., Nolte, D., Mock, A.F., Evidente, V.G., Fee, D.B., Muller, U., et al. (2006). Mutations in voltage-gated potassium channel KCNC3 cause degenerative and developmental central nervous system phenotypes. Nat. Genet. *38*, 447–451.

Wei, A., Covarrubias, M., Butler, A., Baker, K., Pak, M., and Salkoff, L. (1990). K+ current diversity is produced by an extended gene family conserved in Drosophila and mouse. Science *248*, 599–603.

Wolff, M., Casse-Perrot, C., and Dravet, C. (2006). Severe myoclonic epilepsy of infants (Dravet syndrome): natural history and neuropsychological findings. Epilepsia *47* (*Suppl 2*), 45–48.

Wolff, M., Johannesen, K.M., Hedrich, U.B.S., Masnada, S., Rubboli, G., Gardella, E., Lesca, G., Ville, D., Milh, M., Villard, L., et al. (2017). Genetic and phenotypic heterogeneity suggest therapeutic implications in SCN2A-related disorders. Brain *140*, 1316–1336.

Xu, M., Cao, R., Xiao, R., Zhu, M.X., and Gu, C. (2007). The axon-dendrite targeting of Kv3 (Shaw) channels is determined by a targeting motif that associates with the T1 domain and ankyrin G. J. Neurosci. *27*, 14158–14170.

Xu, M., Gu, Y., Barry, J., and Gu, C. (2010). Kinesin I transports tetramerized Kv3 channels through the axon initial segment via direct binding. J. Neurosci. *30*, 15987–16001.

Zhang, Y., Zhang, X.F., Fleming, M.R., Amiri, A., El-Hassar, L., Surguchev, A.A., Hyland, C., Jenkins, D.P., Desai, R., Brown, M.R., et al. (2016). Kv3.3 channels bind Hax-1 and Arp2/3 to assemble a stable local actin network that regulates channel gating. Cell *165*, 434–448.

Zhuchenko, O., Bailey, J., Bonnen, P., Ashizawa, T., Stockton, D.W., Amos, C., Dobyns, W.B., Subramony, S.H., Zoghbi, H.Y., and Lee, C.C. (1997). Autosomal dominant cerebellar ataxia (SCA6) associated with small polyglutamine expansions in the alpha 1A-voltage-dependent calcium channel. Nat. Genet. *15*, 62–69.

ISCI, Volume *9*

Supplemental Information

Balanced Activity between Kv3 and Nav Channels Determines Fast-Spiking in Mammalian Central Neurons

Yuanzheng Gu, Dustin Servello, Zhi Han, Rupa R. Lalchandani, Jun B. Ding, Kun Huang, and Chen Gu

Supplemental Information

Balanced Activity between Kv3 and Nav Channels Determines Fast Spiking in Mammalian Central Neurons

Yuanzheng Gu[1], Dustin Servello[2], Zhi Han[3, 4, 5], Rupa L. Lalchandani[6], Jun B. Ding[6], Ku Huang[3,5,7], and Chen Gu[1,2,*]

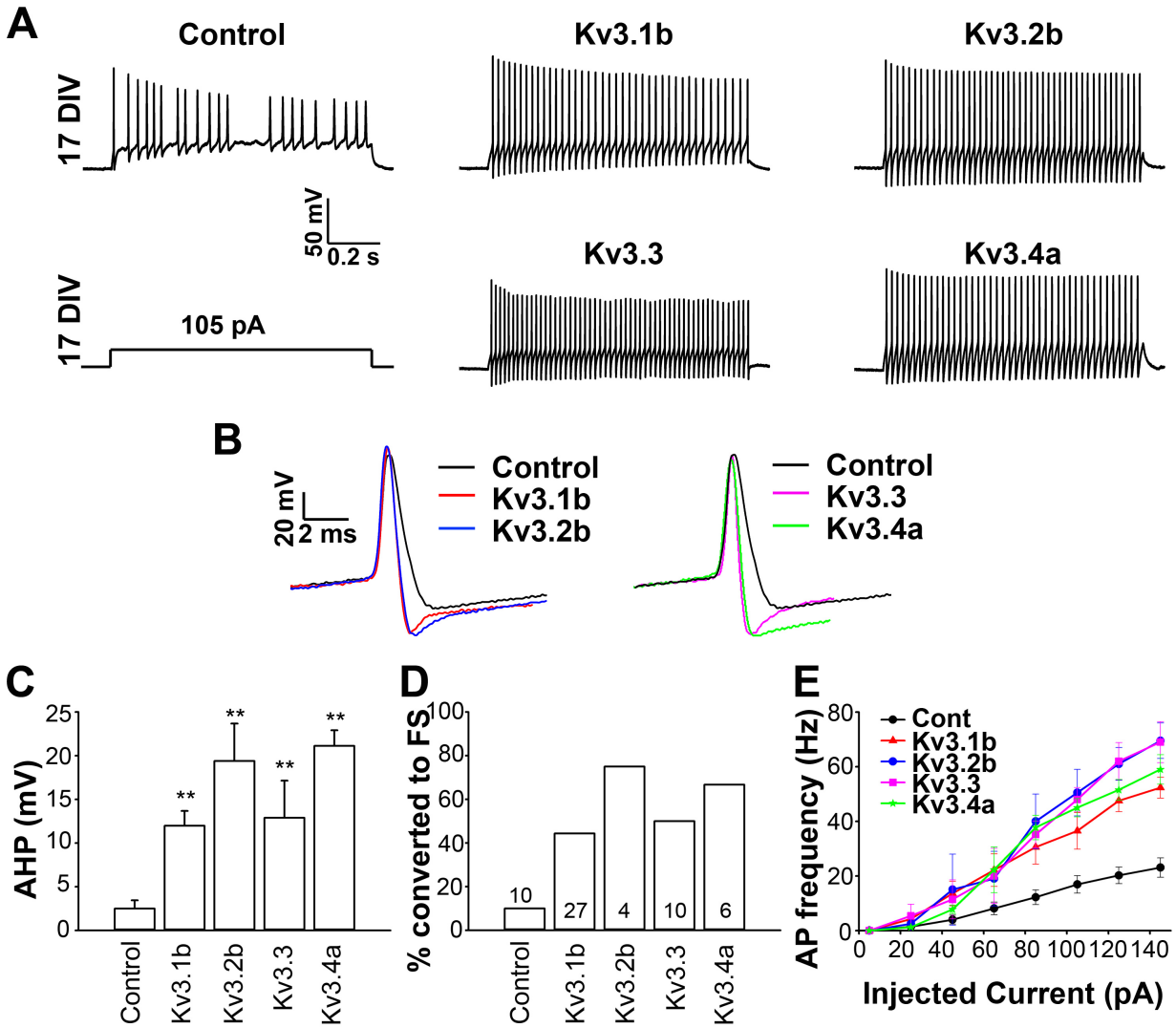

Figure S1. Converting mature SS neurons to FS by different isoforms of Kv3 channels, Related to Figure 1.

(A) Example traces of APs induced by current injection (105 pA; 1 sec) in cultured hippocampal neurons (17 DIV) transfected with different Kv3 constructs.

(B) Waveforms of single APs from transfected mature neurons.

(C)-(E) Summary of the quantification of AP firing recorded from old neurons (17 DIV) transfected with different Kv3 constructs, AHP (C), % neurons converted to FS (D) and the input-output relationship (E). "n" numbers are indicated in (D) and the same in (C) and (E). One-Way ANOVA followed by Dunnett's test was used. **, $p < 0.01$.

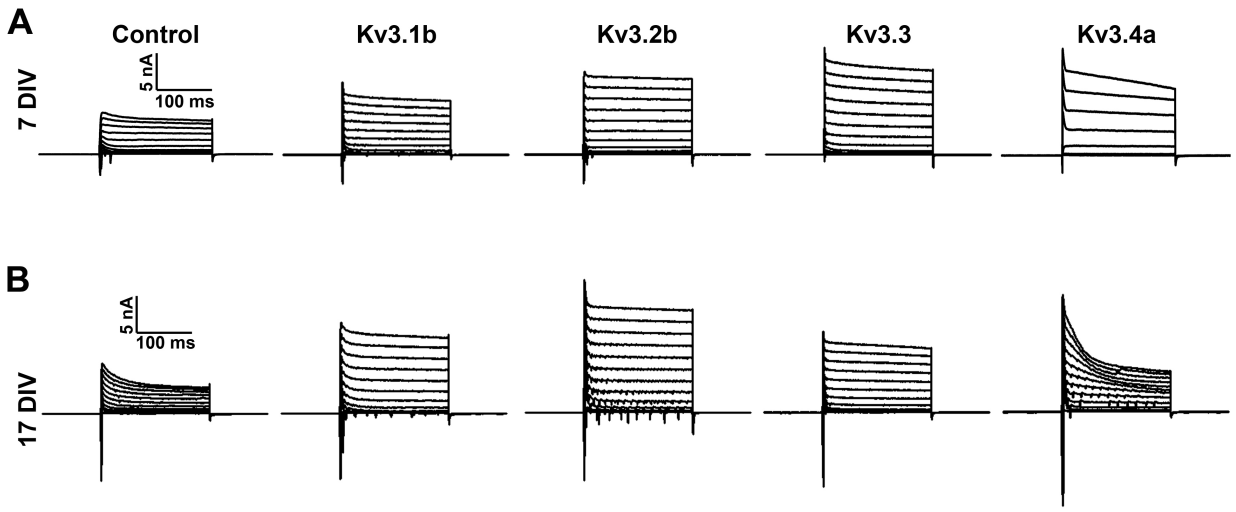

Figure S2. Inward and outward currents from Kv3-transfected neurons, Related Figure 3.

(A) Example traces of voltage-clamp recording from young neurons (7 DIV) transfected with different Kv3 constructs. These are the whole traces corresponding to the ones shown in Figure 3A.

(B) Example traces of voltage-clamp recording from mature neurons (17 DIV) transfected with different Kv3 constructs. These are the whole traces corresponding to the ones shown in Figure 3D.

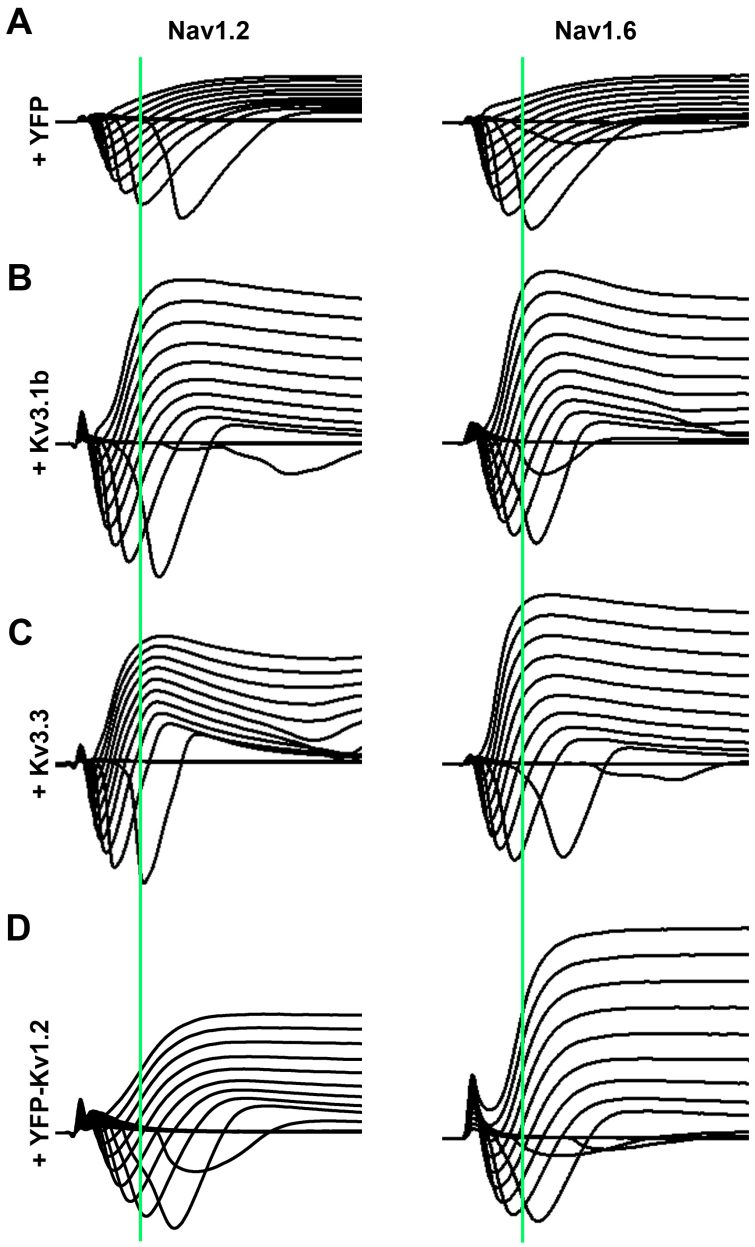

Figure S3. The initial stage of inward and outward currents under voltage-clamp recording from neurons that were transfected with different combination of Nav and Kv channel constructs, Related to Figure 4.

Extended example traces of voltage-clamp (VC) recording (right panels in Figure 4A-H) that were carried out in neurons transfected with Nav1.2 (left) or Nav1.6 (right) with YFP alone (A), or plus Kv3.1b (B), Kv3.3 (C) or YFP-Kv1.2 (D). The total time course is 6 ms.

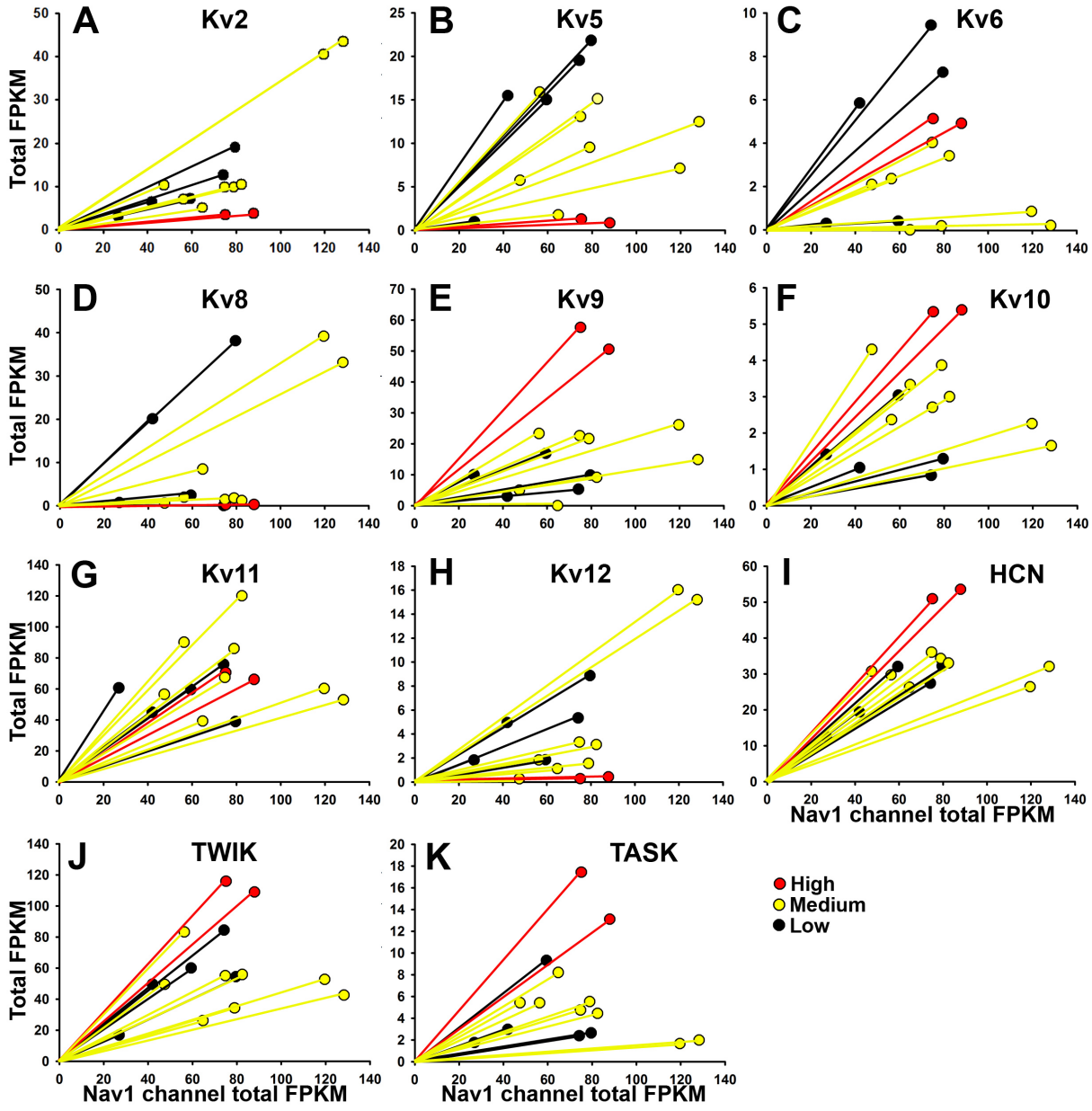

Figure S4. Correlations between K^+ channel subfamilies and Nav1 channel subfamily in different neurons, Related to Figure 7.

Total FPKM of K^+ (and HCN) channel subfamilies (Y) versus the total FPKM of Nav1 channels (X) are plotted for each neuronal type. Red circles: FS neurons. Yellow circles: medium-firing-frequency neurons. Black circles: low-firing-frequency neurons. RNA-seq data sets were obtained from the Allen Institute for Brain Science.

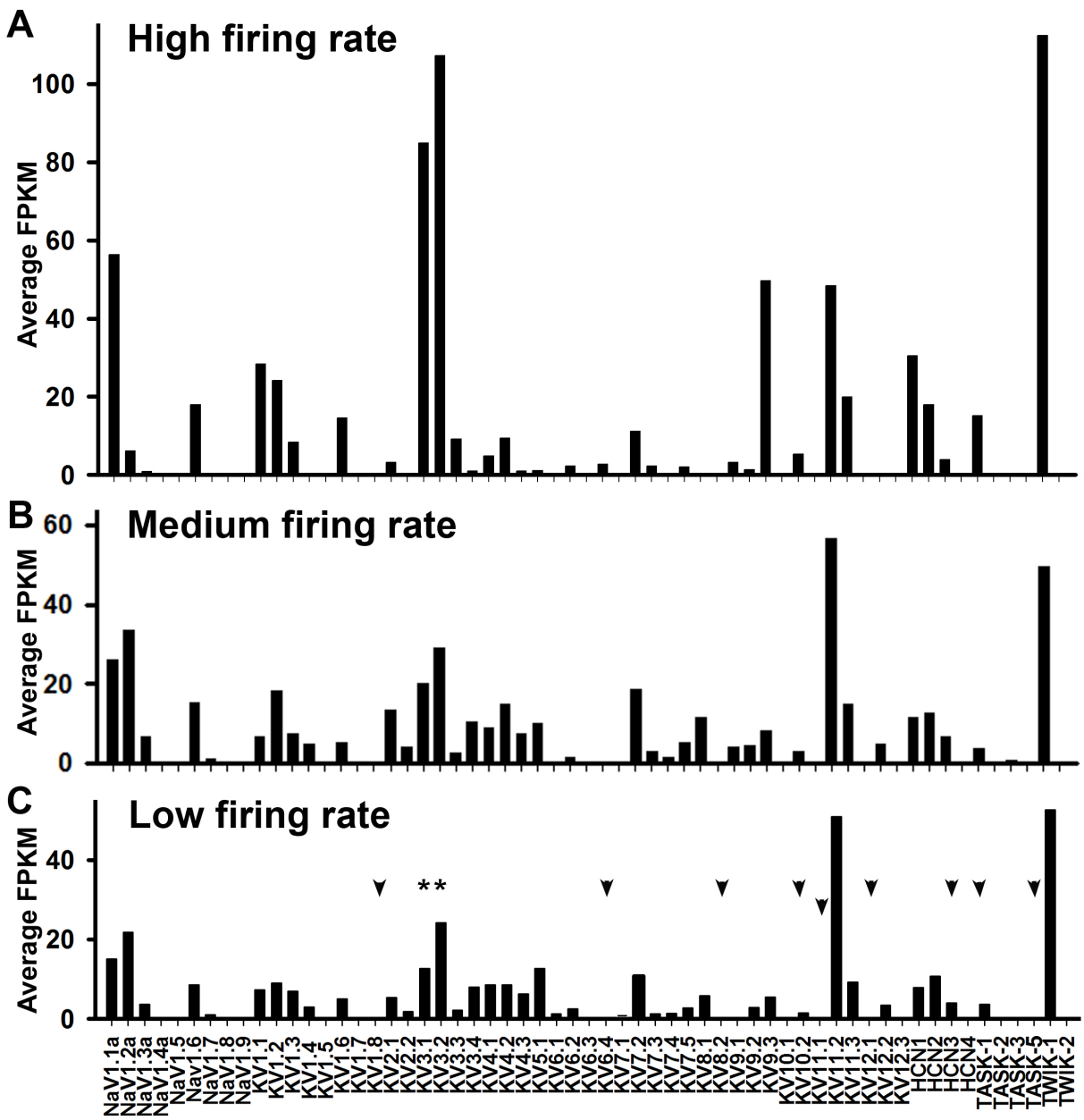

Figure S5. Average mRNA levels of individual Nav1 and K^+ channel genes in the neurons with different firing frequencies, Related to Figure 8.

Neurons are categorized into the following three groups, high firing rate (A), medium firing rate (B) and low firing rate (C). Average FPKM of individual genes (9 Nav1 channel genes, 38 Kv channel genes, 6 two-pore K^+ channel genes and 4 HCN genes) was obtained within each neuron groups. Two best correlations, Kv3.1 and Kv3.2, are indicated with "*". The second tier genes of good correlations are indicated with black arrowheads. RNA-seq data sets were obtained from the Allen Institute for Brain Science.

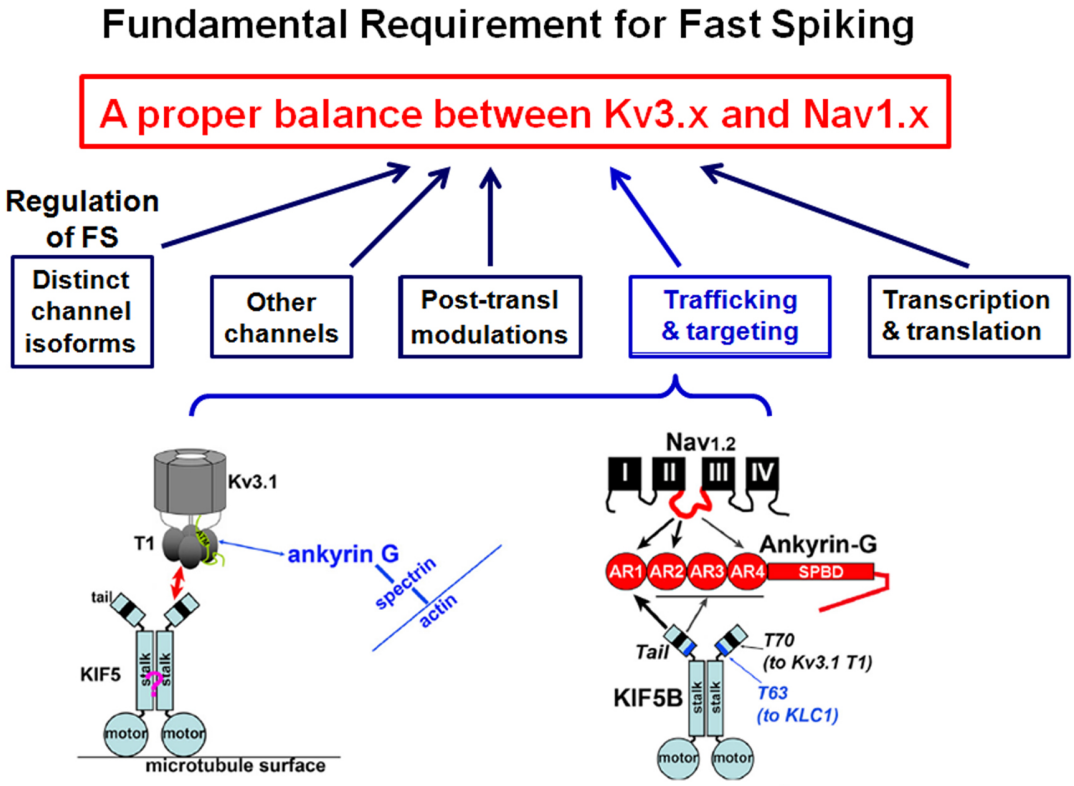

Figure S6. Hypothetical diagram of mechanisms underlying FS induction and regulation in mammalian central neurons, Related to Figure 8.

Kv3.x represents any one isoform of Kv3 channels from Kv3.1 to Kv3.4. Nav1.x represents any one isoform of Nav1 α subunits from Nav1.1 to Nav1.9. FS, fast spiking. T1, the N-terminal tetramerization domain of Kv3.1 channel. KIF5, conventional kinesin heavy chain. The diagram of Kv3.1 transport and targeting (the lower left panel) is from our previous paper (Xu et al., 2010). KIF5B is one of the three isoforms of KIF5 proteins (KIF5A, KIF5B and KIF5C). The diagram of Nav1.2 channel transport and targeting (the lower right panel) is from our recent paper (Barry et al., 2014).

gene_id	gene_entrez_id	gene_symbol	gene_name
500715342	16485	Kcna1	Kv1.1
500707406	242151	Kcna2	Kv1.2
500707405	16490	Kcna3	Kv1.3
500707402	16491	Kcna4	Kv1.4
500704262	16492	Kcna5	Kv1.5
500715338	16493	Kcna6	Kv1.6
500715343	16494	Kcna7	Kv1.7
500717470	16495	Kcna10	Kv1.8
500705479	16500	Kcnb1	Kv2.1
500699796	98741	Kcnb2	Kv2.2
500717525	16502	Kcnc1	Kv3.1
500725744	268345	Kcnc2	Kv3.2
500717401	16504	Kcnc3	Kv3.3
500707416	99738	Kcnc4	Kv3.4
500742892	16506	Kcnd1	Kv4.1
500713405	16508	Kcnd2	Kv4.2
500707369	56543	Kcnd3	Kv4.3
500729179	382571	Kcnf1	Kv5.1
500705523	241794	Kcng1	Kv6.1
500741394	240444	Kcng2	Kv6.2
500740111	225030	Kcng3	Kv6.3
500721492	66733	Kcng4	Kv6.4
500719509	16535	Kcnq1	Kv7.1
500705819	16536	Kcnq2	Kv7.2
500735801	110862	Kcnq3	Kv7.3
500709676	60613	Kcnq4	Kv7.4
500699876	226922	Kcnq5	Kv7.5
500735618	67498	Kcnv1	Kv8.1
500742177	240595	Kcnv2	Kv8.2
500705368	16538	Kcns1	Kv9.1
500735465	16539	Kcns2	Kv9.2
500729103	238076	Kcns3	Kv9.3
500702292	16510	Kcnh1	Kv10.1
500729889	238271	Kcnh5	Kv10.2
500710976	16511	Kcnh2	Kv11.1
500728564	192775	Kcnh6	Kv11.2
500703357	170738	Kcnh7	Kv11.3
500739679	211468	Kcnh8	Kv12.1
500736623	16512	Kcnh3	Kv12.2

500728369	380728	Kcnh4	Kv12.3
500721734	16525	Kcnk1	TWIK1
500716903	52150	Kcnk6	TWIK2
500711115	16527	Kcnk3	TASK1
500733334	16529	Kcnk5	TASK2
500703382	20265	Scn1a	Nav1.1a
500703377	110876	Scn2a1	Nav1.2a
500703375	20269	Scn3a	Nav1.3a
500728578	110880	Scn4a	Nav1.4a
500723949	20271	Scn5a	Nav1.5a
500736693	20273	Scn8a	Nav1.6a
500703386	20274	Scn9a	Nav1.7a
500723950	20264	Scn10a	Nav1.8a
500723952	24046	Scn11a	Nav1.9a
500717017	20266	Scn1b	Nav1.1b
500722556	72821	Scn2b	Nav2.1b
500722419	235281	Scn3b	Nav3.1b
500722557	399548	Scn4b	Nav4.1b
500733003	15165	Hcn1	HCN1
500725164	15166	Hcn2	HCN2
500706861	15168	Hcn3	HCN3
500722844	330953	Hcn4	HCN4

Table S1. The list of genes included in the bioinformatics analysis, Related to Figure 7.

Transparent Methods

cDNA constructs

Kv3.1bHA and Kv3.1aHA was constructed by inserting an HA tag (YPYDVPDYA) into the first extracellular loop right behind T231 (Xu et al., 2007). Mouse Kv3.2b was purchased from Invitrogen. Human Kv3.3 was a kind gift from Dr. James L Rae and previously published (Rae and Shepard, 2000). Kv3.4a was kindly provided by Dr. Tatiana Tkatch. Kv3.4aHA was constructed by inserting an HA tag (YPYDVPDYA) into the first extracellular loop right behind S269. Nav1.2-GFP was kindly provided by Dr. Alan Goldin and previously published (Barry et al., 2014). Mouse Nav1.6 was kindly provided by Dr. Theodore R. Cummins.

Whole-cell recording from brain slices

Coronal sections (300 μm in thickness) were cut from p15-p18 wild type, SST-Cre;Ai9 and PV-Cre;Ai9 mice. SST+ and PV+ interneurons, were identified with fluorescence. Whole-cell recording was performed initially at the current-clamp mode, followed by the voltage-clamp recording, in the presence of aCSF with 1 μM TTX, 5 μM NBQX, 5 μM CPP, 50 μM picrotoxin. The recording was carried out at room temperature. Recording pipettes (3–5MΩ) were filled with a K internal solution consisting of (in mM) 135 KMeSO4, 5 KCl, 0.5 CaCl2, 5 HEPES, 5 EGTA, 2 Mg-ATP, and 0.3 Na-GTP, pH 7.3 adjusted with KOH. In the current-clamp mode, injected currents (2000 ms duration) were from -200 pA to 340 pA in a 90-pA-increment. In the voltage-clamp mode, voltage episodes (1000 ms duration) were applied from -80 mV to +60 mV with a 10-mV-increment, holding potential at -70 mV and a pre-pulse at -100 mV (250 ms duration).

Primary hippocampal neuron cultures

All animal experiments were conducted in accordance with the NIH Animal Use Guidelines and Institutional Animal Care and Use Committee (IACUC) of the Ohio State University. The E18 hippocampal neuron culture was prepared as previously described from rat hippocampi at the embryonic day 18 (E18) (Barry et al., 2014; Gu et al., 2006; Gu et al., 2012; Gu and Gu, 2010). For transient transfection, neurons in culture at 5 DIV (young) were incubated in Opti-MEM containing 0.8 μg of cDNA plasmid and 1.5 μl of Lipofectamine2000 (Invitrogen, Carlsbad, CA, USA) for 20 min at 37°C.

More mature neurons (15 DIV) in culture were transfected with the Ca^{2+}/phosphate method, which was described in our previous studies (Barry et al., 2014). In brief, cDNA/Ca^{2+} solution (1 μg cDNA, 3.1 μl 2M $CaCl_2$, up to 25 μl ddH_2O) was added to 25 μl 2xHBS (136.9 mM NaCl, 1.5 mM $Na_2PO_4 \cdot 7H_2O$, 26 mM HEPES, pH 7.05), and incubated together at room

temperature for 20 min. Then 0.5 ml medium was removed from 1 well of 24 well plate and placed together with 20-30% maintenance media (of 0.5 ml) at 37°C 10% CO2 for 15 min. The cDNA mixture was added to the well and incubated for 1 h at 37°C in 5% CO2. Media were removed and then replaced with the 10% CO2 equilibrated buffer.

Current- and voltage-clamp recording from cultured neurons

Glass pipettes with tip diameter around 1 μm and resistance of 2-3 MΩ for whole-cell recording were pulled with Model P-1000 Flaming/Brown micropipette puller (Sutter Instrument, Novato, CA, USA). Both mature neurons (~ 16DIV) and young neurons (~ 7 DIV) transfected with interesting constructs were recorded. The current-clamp procedure was previous described (Gu et al., 2012). Action potentials induced by current injection from the recording pipette were recorded under the current-clamp mode. The membrane resistance, capacitance, and resting membrane potentials of the neurons were measured. These values are consistent within each age group. For long pulse stimulations, 1000-ms duration currents of increasing amplitude (from 5 to 145 pA with increments of 10 pA) were injected. Due to the variation of expression levels of transfected channel constructs, only the neurons carrying clear after-hyperpolarization were used for quantification of spiking frequency. For voltage-clamp recording, the membrane potential of the cultured neurons was held at -80 mV, a series of 20-ms voltage episodes from -60 mV to +60 mV with increments in 10 mV was applied to neurons. The internal solution and Hank's buffer were previously described for recording of primary cultured neurons (Gu et al., 2012; Gu et al., 2013). Hank's buffer: 150 mM NaCl, 4 mM KCl, 1.2 mM $MgCl_2$, 10 mg/ml glucose, 1 mM $CaCl_2$, 20 mM HEPES (pH 7.4). The internal solution of electrical pipettes: (in mM) 122 $KMeSO_4$, 20 NaCl, 5 Mg-ATP, 0.3 GTP and 10 HEPES (pH 7.2).

Voltage-clamp recording from transfected HEK293 cells

Biophysical properties of various Kv3 channel constructs were determined with voltage clamp recording on transfected HEK293 cells with the same internal solution and Hank's buffer, as previously described (Gu et al., 2012; Gu et al., 2013). Conductance-voltage relationships (G-V curves) for Kv channel constructs were $G = I / (V_m - V_{rev})$, V_{rev} = -95 mV, normalized to the maximal conductance. Curves were fitted with Boltzmann function, $G/G_{max}=1/(1+\exp[-(V-V_{1/2})/k])$, where G_{max} is the maximal conductance, $V_{1/2}$ is the potential at which the value of the relative conductance is 0.5, and k is the slope factor. SigmaPlot 10.0 (Systat Software, Inc., Chicago, IL, USA) was used for fitting. To obtain activation time constant (τ_{on}), activation curves (at +30 mV) were fitted with a single exponential function raised to a power of 4, $I(t)=A(1-\exp(-$

$t/\tau_{on}))^4$. In studies of deactivation kinetics of Kv channels, the cells were held at -80 mV, given a 2-ms pre-pulse to +60 mV and 20-ms voltage episodes from -100 mV to -10 mV. To obtain deactivation time constant (τ_{off}), tail currents (at -60 mV) were fitted with the equation, $I(t)=Aexp(-t/\tau_{off})$. Clampfit 10.0 was used for fitting to get τ_{on} and τ_{off}.

Antibodies

Antibodies used include the following: rat monoclonal anti-HA antibody (Roche, Indianapolis, IN), rabbit anti-Kv3.1b, Kv3.2, Kv3.3 and Kv3.4 antibodies (Alomone Labs), mouse anti-AnkG antibody (NeuroMab UC Davis clone N106/36), mouse anti-Nav1.2 antibody (NeuroMab UC Davis clone K69/3), mouse anti-pan-Nav channel (Sigma-Aldrich, St Louis, MO, USA), and Cy2-, Cy3- and Cy5-conjugated secondary antibodies (Jackson ImmunoResearch Laboratories, West Grove, PA, USA).

Immunostaining, imaging and quantification

The immunocytochemical procedures were previously described (Gu et al., 2006; Xu et al., 2007). Briefly, neurons were stained under the non-permeabilized condition (without Triton X100) to label the surface pool and under the permeabilized condition (with 0.2% Triton X100) to label total proteins. Fluorescence images were captured with a Spot CCD camera RT slider (Diagnostic Instrument Inc., Sterling Heights, MI) in a Zeiss upright microscope, Axiophot, using Plan Apo objectives 20×/0.75 and 100×/1.4 oil, saved as 16-bit TIFF files, and analyzed with NIH Image J and Sigmaplot 10.0 for fluorescence intensity quantification. The quantification procedure was also described previously (Xu et al., 2007; Xu et al., 2010).

shRNA knockdown of endogenous AnkG

Construction and validation of vector-based short interfering RNA (siRNA) strategy to suppress the levels of endogenous AnkG in rat hippocampal neurons were previously described (Barry et al., 2014; Xu et al., 2007). We used the previously generated AnkG siRNA construct made from insertion of a sense and antisense loop of AnkG (21 nucleotides) into pRNAT-H1.1/neo vector (GenScript, Piscataway, NJ, USA). The GFP coding region in the vector was replaced with the coding sequence for mCherry between BamH1 and HindIII sites. Therefore, the neurons transfected with the siRNA plasmid expressed mCherry as the indicator for transfection. The siRNA plasmid was transfected into neurons at 5 DIV and the neurons were recorded both in current and voltage clamp modes 5-6 days after transfection.

Bioinformatics of RNA sequence data analysis

RNAseq data was obtained from the Allen Institute's Allen Brain Atlas Data Portal (http://celltypes.brain-map.org/rnaseq, all sequencing methods can be obtained from the "Documentation" tab at the link provided). For each individual gene, FPKM values were averaged for individual cell types corresponding to unique drivers (Lateral geniculate nucleus: Gad2-IRES-Cre. Primary visual cortex: *Gad2*-IRES-Cre, *Pvalb*-IRES-Cre, *Sst*-IRES-FlpO, *Scnn1a*-Tg2-Cre, *Ctgf*-2A-dgCre, *Ndnf*-IRES2-dgCre, *Rbp4*-Cre_KL100, *Chrna2*-Cre_OE25, *Chat*-IRES-Cre, *Nr5a1*-Cre and *Vip*-IRES-Cre. Anterior lateral motor area: *Htr3a*-Cre_NO152, *Sst*-IRES-FlpO and *Pvalb*-IRES-Cre). Gene ID for each channel is available in Table 1 in the Supplementary Information.

Firing rate data was obtained from the Allen Institute's Allen Brain Atlas Data Portal (http://celltypes.brain-map.org/mouse/data) as well as matched with directly corresponding or spatially similarly located brain regions from peer-reviewed literature. Firing rates obtained from the Allen institute included primary visual cortex (*Gad2*-IRES-Cre, *Pvalb*-IRES-Cre, *Sst*-IRES-FlpO, *Scnn1a-Tg2*-Cre, *Ctgf*-2A-dgCre, *Ndnf*-IRES2-dgCre, *Rbp4*-Cre_KL100, *Chrna2*-Cre_OE25, *Chat*-IRES-Cre, *Nr5a1*-Cre and *Vip*-IRES-Cre). Literature based firing rates included lateral geniculate nucleus (*Gad2*-IRES-Cre) anterior lateral motor area (*Htr3a*-Cre_NO152, *Sst*-IRES-FlpO, and *Pvalb*-IRES-Cre). Max firing rate data was averaged according to individual drivers. Cell types were grouped into four groups based on their firing rate according to literature that had previously identified specific cell drivers being expressed in neurons of either high, medium (regular), or low firing rates (Hilscher et al., 2017; Karnani et al., 2013; Lee et al., 2010; Levy and Reyes, 2012; Mastro et al., 2014; Sotty et al., 2003; Tyan et al., 2014).

A similar division strategy was utilized for fast and regular spiking neurons (Subkhankulova et al., 2010). If the firing rate type had not been determined previously, firing rate type was assigned to produce an even distribution of firing rates with at least n=3 per group, except for the high firing rate neurons as they are only represented by the same cell type. The group ranges for firing rates were: high (>250 Hz, *Pvalb*-IRES-CRE from the primary visual cortex and anterior lateral motor area), medium high (100-250 Hz, lateral geniculate nucleus: *Gad2*-IRES-Cre; primary visual cortex: *Gad2*-IRES-Cre *Sst*-IRES-FlpO, *Scnn1a*-Tg2-Cre, and *Vip*-IRES-Cre), medium (70-100 Hz, *Nr5a1*-Cre and, and Anterior Lateral Motor Area: *Htr3a*-Cre_NO152 and *Sst*-IRES-FlpO), and low (<70 Hz, primary visual cortex: *Ctgf*-2A-dgCre, *Ndnf*-IRES2-dgCre, *Rbp4*-Cre_KL100, *Chrna2*-Cre_OE25, *Chat*-IRES-Cre,). For absolute

transcript level analysis three groups were used: high, medium (combining medium and medium high), and low.

Statistical analysis

Results were presented as the mean ± SEM. Two-tailed Student's t-test was used for comparisons between two groups. One-way ANOVA followed by Dunnett's test was used for comparing two or more groups to one control group. (*) $p < 0.05$, (**) $p < 0.01$ and (***) $p < 0.001$ were considered statistically significant.

Supplemental References

Barry, J., Gu, Y., Jukkola, P., O'Neill, B., Gu, H., Mohler, P.J., Rajamani, K.T., and Gu, C. (2014). Ankyrin-G directly binds to kinesin-1 to transport voltage-gated Na+ channels into axons. Developmental Cell *28*, 117-131.

Gu, C., Zhou, W., Puthenveedu, M.A., Xu, M., Jan, Y.N., and Jan, L.Y. (2006). The microtubule plus-end tracking protein EB1 is required for Kv1 voltage-gated K+ channel axonal targeting. Neuron *52*, 803-816.

Gu, Y., Barry, J., McDougel, R., Terman, D., and Gu, C. (2012). Alternative splicing regulates kv3.1 polarized targeting to adjust maximal spiking frequency. Journal of Biological Chemistry *287*, 1755-1769.

Gu, Y., Barry, J., and Gu, C. (2013). Kv3 channel assembly, trafficking and activity are regulated by zinc through different binding sites. The Journal of physiology *591*, 2475-2490.

Gu, Y., and Gu, C. (2010). Dynamics of Kv1 channel transport in axons. PLoS One *5*, e11931.

Hilscher, M.M., Leao, R.N., Edwards, S.J., Leao, K.E., and Kullander, K. (2017). Chrna2-Martinotti Cells Synchronize Layer 5 Type A Pyramidal Cells via Rebound Excitation. PLoS biology *15*, e2001392.

Karnani, M.M., Szabo, G., Erdelyi, F., and Burdakov, D. (2013). Lateral hypothalamic GAD65 neurons are spontaneously firing and distinct from orexin- and melanin-concentrating hormone neurons. The Journal of physiology *591*, 933-953.

Lee, S., Hjerling-Leffler, J., Zagha, E., Fishell, G., and Rudy, B. (2010). The largest group of superficial neocortical GABAergic interneurons expresses ionotropic serotonin receptors. J Neurosci *30*, 16796-16808.

Levy, R.B., and Reyes, A.D. (2012). Spatial profile of excitatory and inhibitory synaptic connectivity in mouse primary auditory cortex. J Neurosci *32*, 5609-5619.

Mastro, K.J., Bouchard, R.S., Holt, H.A., and Gittis, A.H. (2014). Transgenic mouse lines subdivide external segment of the globus pallidus (GPe) neurons and reveal distinct GPe output pathways. J Neurosci *34*, 2087-2099.

Rae, J.L., and Shepard, A.R. (2000). Kv3.3 potassium channels in lens epithelium and corneal endothelium. Exp Eye Res *70*, 339-348.

Sotty, F., Danik, M., Manseau, F., Laplante, F., Quirion, R., and Williams, S. (2003). Distinct electrophysiological properties of glutamatergic, cholinergic and GABAergic rat septohippocampal neurons: novel implications for hippocampal rhythmicity. The Journal of physiology *551*, 927-943.

Subkhankulova, T., Yano, K, Robinson, H.P., and Livesey, F.J. (2010). Grouping and classifying electrophysiologically-defined classes of neocortical neurons by single cell, whole-genome expression profiling. Front Mol Neurosci *3*,10.

Tyan, L., Chamberland, S., Magnin, E., Camire, O., Francavilla, R., David, L.S., Deisseroth, K., and Topolnik, L. (2014). Dendritic inhibition provided by interneuron-specific cells controls the firing rate and timing of the hippocampal feedback inhibitory circuitry. J Neurosci *34*, 4534-4547.

Xu, M., Cao, R., Xiao, R., Zhu, M.X., and Gu, C. (2007). The axon-dendrite targeting of Kv3 (Shaw) channels is determined by a targeting motif that associates with the T1 domain and ankyrin G. J Neurosci *27*, 14158-14170.

Xu, M., Gu, Y., Barry, J., and Gu, C. (2010). Kinesin I transports tetramerized Kv3 channels through the axon initial segment via direct binding. J Neurosci *30*, 15987-16001.